



## Supplementary Materials for

### **Aging Fly Cell Atlas identifies exhaustive aging features at cellular resolution**

Tzu-Chiao Lu *et al.*

Corresponding authors: Heinrich Jasper, jasperh@gene.com; Stephen R. Quake, steve@quake-lab.org; Hongjie Li, hongjie.li@bcm.edu

*Science* **380**, eadg0934 (2023)  
DOI: 10.1126/science.adg0934

#### **The PDF file includes:**

Materials and Methods  
Figs. S1 to S30  
References

#### **Other Supplementary Material for this manuscript includes the following:**

Movies S1 to S3  
MDAR Reproducibility Checklist

## Materials and Methods

### Fly sample and lifespan

Fly head and body samples were from F1 of two wild type fly stains: female *w<sup>1118</sup>* and male Oregon R (*OreR*). Flies were maintained on standard cornmeal medium at 25 °C with 12-hour light–dark cycle. For the lifespan experiment, progenies were collected 3 days after the first fly hatched. Flies were allowed to mate for 3 days. Then male and female flies were separated into different cages (120 flies per cage) for lifespan or sample collection at 25°C. Fly food was changed every 2 days. Dead flies were counted every 2 days. Lifespan curves were generated in Excel.

### Single-nucleus RNA sequencing

Fly heads and bodies dissected at different ages were put into 1.5ml RNAase-free Eppendorf tubes, flash-frozen in liquid nitrogen, and then stored at –80 °C. We put 100 heads or 50 bodies in each tube. Single-nucleus suspensions were prepared following the protocol described in the Fly Cell Atlas study (7). Next, we collect nuclei by FACS. We used the SONY SH800 FACS sorter for collecting nuclei. Nuclei were stained by Hoechst-33342 (1:1000; >5min). Since polyploidy is common for many fly tissues, we observed different populations of nuclei according to DNA content (Hoechst signal). In order to include all cell populations with different nuclear sizes, we have included all nuclear populations from the FACS. Nuclei were collected into a 1.5ml tube with 200ul 1x PBS with 0.5% BSA as the receiving buffer (RNase inhibitor added). For each 10x Genomics run, 100k–400k nuclei were collected. Nuclei were spun down for 10 min at 1000g at 4 °C and then resuspended using 40ul or desired amount of 1x PBS with 0.5% BSA (RNase inhibitor added). 2ul nucleus suspension was used for counting the nuclei with hemocytometers to calculate the concentration. When loading to the 10x controller, we always target 10k nuclei for each channel. We observed that loading 1.5 folds more nuclei as recommended by the protocol allowed us to recover about 10k cells after sequencing. For example, if the concentration is 1500 nuclei per ul for one sample, we treat it as 1000 nuclei per ul when loading to the 10x controller.

Next, we performed snRNA-seq using the 10x Genomics system with 3' v3.1 kits with the following settings. All PCR reactions were performed using the Biorad C1000 Touch Thermal cycler with 96-Deep Well Reaction Module. 13 cycles were used for cDNA amplification and 16 cycles were used for sample index PCR. As per 10x protocol, 1:10 dilutions of amplified cDNA and final libraries were evaluated on a bioanalyzer. Each library was diluted to 4 nM, and equal volumes of 18 libraries were pooled for each NovaSeq S4 sequencing run. Pools were sequenced using 100 cycle run kits and the Single Index configuration. Read 1, Index 1 (i7), and Read 2 are 28 bp, 8 bp and 91 bp respectively. A PhiX control library was spiked in at 0.2 to 1% concentration. Libraries were sequenced on the NovaSeq 6000 Sequencing System (Illumina).

For each age, we sequenced the head for 12 runs (6 for male and 6 for female) and body for 12 runs (6 for male and 6 for female). To collect enough nuclei for 6 runs, we used 100 heads and 50 bodies. For three ages, we sequenced 24\*3 = 72 runs. We have recently published a protocol describing the single-nucleus RNAseq in *Drosophila* and all the above steps have been detailed (54).

## **Sequencing read alignment**

The raw FASTQ files were first filtered for the index-hopping reads by using the index-hopping-filter developed by the 10x Genomics (version 1.0.1). Before mapping reads, the *Drosophila melanogaster* genome (FlyBase r6.31) was indexed with a pre-mRNA GTF, which was established by FCA (7), using the Cell Ranger (version 4.0.0). FASTQ files removing the index-hopping reads were mapped to the *Drosophila melanogaster* genome (r6.31) using Cell Ranger Count (version 4.0.0) to generate the count matrix.

## **AFCA annotation**

In the FCA dataset, there are 251 cell types annotated, many of which were characterized in dissected tissues. For cell types from the head, besides the whole head sequencing, there are only two dissected tissues: antennae and proboscis. So, most cell types from the aging head can be annotated based on the FCA whole head data. For cell types from the body, most cell type annotations are from tissues (only 33 annotated cell types from the FCA whole-body data). To annotate aging body data, we need to transfer annotations from the body and individual tissues (e.g., gut, wing, leg, testis, ovary, fat body, etc). Thus, the aging head and body data were annotated using slightly different strategies and we characterized them separately. For both, we first integrated FCA and AFCA datasets and corrected age and sex differences using Harmony (55). Next, we characterized cell types using two different approaches: co-clustering and supervised machine learning (ML)-based classification. Then, we validated those two approaches using cell type-specific markers and performed manual correction when necessary.

For the head data, FCA and AFCA head cells were co-clustered and 150 principal components (PCs) were selected for clustering. We followed the co-cluster-based approaches utilized in FCA brain-head integration (7) and annotations from the FCA cells were transferred to the clusters that contained at least 15% of cells with the same annotation. Alternatively, if more than 15% of the annotation-specific cells were enriched in the clusters, those clusters were assigned to the corresponding annotations. Different Leiden resolutions were applied for the transfer and the one with the maximum number of transferred annotations was chosen. If annotations from the two approaches were not consistent, cluster-dominant annotations would be assigned to the clusters. Besides cluster-based transfer, we also included a supervised ML method. We utilized the Logistic Regression classifier to transfer the FCA annotations to AFCA cells. FCA cells were used as the training dataset, while AFCA samples were considered as test data. By comparing the annotations from these two approaches, annotations were manually confirmed by examining the expression of cell type-specific genes to prevent the loss of transfer due to aging. Also, annotations were unified and denoised at the cluster level. In total, 91 cell types were annotated, including 17 newly identified neuron types.

To annotate AFCA body cells, FCA and AFCA body cells were first co-clustered using 50 PCs and 33 annotations from the FCA body were transferred to the AFCA body cells using approaches similar to the head transfer. To include annotations from different body tissues, we co-clustered

cells from the FCA body, AFCA body, and all FCA tissues to identify clusters with tissue-specific annotations (**Fig. S4**). The cluster-based method enabled us to quickly identify tissue-specific annotations from integrated body and tissue cells. Clusters with tissue-specific annotations were chosen for further sub-clustering and tissue annotations were transferred similarly using cluster- and supervised ML-based approaches. Due to the similarity between some gut and malpighian tubule cell types, especially for the intestinal stem cell and renal stem cell (**Fig. S6C and S7**), we combined annotations from these two tissues together for the transfer. Some cell types, like muscle cells, were present in multiple tissues and we considered subsetting those cells based on the expression of cell-type markers, instead of selecting the annotation-enriched clusters (**Fig. S5**). After subsetting marker-positive cells, FCA annotations were similarly transferred. After transferring all tissue annotations, 72 cell types were annotated in the AFCA body.

### Gut cell type case study

The analysis of the gut cells in the AFCA data was performed using SCANPY and scFates python packages (56, 57). The intestinal stem cell lineage was isolated from the data and includes intestinal stem cells, enteroblasts, adult differentiating enterocytes, enteroendocrine cells, anterior enterocytes, and posterior enterocytes. The pseudotime was generated by combining the young (FCA age 5d sample) and old (AFCA age 50d and 70d samples). To generate this plot, the partition-based graph abstraction (PAGA) function was applied to infer the connectivity of clusters then the ForceAtlas2 algorithm was implemented to spatially overlay the cells onto the connectivity plot generated by PAGA (16, 17). To compare the cell compositions of each age, the cells of different ages were plotted separately next to the pseudotime. The percentages of cells comprising the intestinal stem cell lineage were extracted from the data and then plotted in **Fig 2D**.

The changes in gene expression were generated using the scFates python package (57). Cells were isolated from each age and then run separately in the scFates pipeline. Briefly, scFates uses the EIPiGraph algorithm to learn the topography of the data. Then, the pseudotime was constructed from the graph inferred by the EIPiGraph algorithm. The genes differentially expressed along the trajectory were determined using a cubic spline regression model and then these results were compared to an unrestrained model. The Benjamini-Hochberg correction was then applied to adjust for multiple comparisons. A significantly altered gene along the trajectory between each age, Rbfox1, is shown in **Fig S11**.

### Fat body and indirect flight muscle staining

To label the fat body tissue with GFP, cg-GAL4 (Bloomington Drosophila Stock Center (BDSC), #7011) virgins were crossed with UAS-unc84GFP (from Dr. Gilbert L. Henry) or UAS-CD8GFP (from Dr. Liqun Luo) males to obtain cg-GAL4>unc84GFP or cg-GAL4>CD8GFP flies. For indirect flight muscle labeling, Act88F-GAL4 (BDSC #38461) virgins were crossed with UAS-unc84GFP to obtain Act88F-GAL4>unc84GFP flies. Flies were cultured at 25°C to desired ages.

For fat body dissection, fly abdomen filets were prepared in 1X PBS using Vannas Spring Scissors (FST, 3mm Cutting Edge, 15000-00) and Dumont #55 forceps (FST, 11255-20). For indirect flight

muscle dissection, flies in 1.5ml Eppendorfs tube were snap-freezed in liquid nitrogen and placed on the ice rack. After removing the head, leg, and wing, the abdomen was clamped with forceps and the thorax was cut in the sagittal section by a razor. Tissues were fixed with 4% paraformaldehyde for 20 min at room temperature (RT), washed with 1X PBS, blocked in 5% NGS blocking buffer (1XPBS, 0.3% Triton X-100, 5% NGS) for 2 h at RT, incubated with primary antibodies (in 5% NGS blocking buffer) overnight at 4°C, and then washed 5 times with 0.3% PBST (1XPBS, 0.3% Triton X-100) before incubation with secondary antibodies for 2 h at RT. Tissues were thoroughly rinsed in PBST, stained with DAPI(1:1000) for 15 min, washed with 1XPBS and mounted with SlowFade™ Gold Antifade Mountant (Thermo Fisher, S36936).

Mouse anti-LamC (1:100, Developmental Studies Hybridoma Bank (DSHB), LC28.26), chicken anti-GFP (1:1000, Aves Labs), rabbit anti-pH3 (1:1000, Cell Signaling Technology, #9701), rabbit anti-cleaved-Caspase3 (1:100, Cell Signaling Technology, #9661) were used as primary antibodies. For secondary antibodies, we used Cy™3 AffiniPure Donkey Anti-Mouse IgG (H+L) (1:250, Jackson ImmunoResearch, AB\_2340813), Alexa Fluor® 488 AffiniPure Donkey Anti-Chicken IgY (IgG) (H+L) (1:250, Jackson ImmunoResearch, AB\_2340375), Alexa Fluor™ 647 Donkey anti-Rabbit IgG (H+L) Highly Cross-Adsorbed Secondary Antibody (1:250, Invitrogen, A31573). Alexa Fluor 647 Phalloidin (1:250, Invitrogen, A22287) was used to stain F-actin in muscle.

Images were obtained with Leica STELLARIS 5 confocal microscope. Images were obtained as Z series with the same interval. Z series images were merged by ImageJ (Image-Stacks-Z projection-Max Intensity), and then the mean fluorescence intensity was measured (Analyze-Measure-Mean gray value) or the nuclear number was counted by Point Tool. Quantification graphs are generated by GraphPad Prism. P-values from unpaired t-test. Error bar, SD.

### **DEG analysis**

To identify genes that are differentially expressed in the aged population, we applied the Wilcoxon Rank Sum test (rank\_genes\_groups() in SCANPY) to compare the gene expression between the aged (30d, 50d, and 70d) and the young population (5d). Genes with FDR lower than 0.05 would be considered to be differentially expressed.

### **Change of cell composition**

Cell numbers of each cell type were counted and separated by age. To get the ratio of one cell type from one age, the cell numbers of a specific cell type and age were further divided by the total cell number of the corresponding age. The cell-type ratios from the aged population (30d, 50d, 70d) were further divided by ratios from the young population (5d) to get the relative ratios in the log2 scale.

### **GO analysis**

In each cell type, aging DEGs, including up- or down-regulated genes, were applied for the Gene Ontology (GO) analysis using GOATOOLS (version 1.2.3) (58). The gene association file (version FB2022\_04) was downloaded from FlyBase. Redundant GO terms were removed by REVIGO

(59). GO terms from Biological Process (BP) were mainly used for our analysis (**Fig. 3E and 3F**). GOs restricted within 5 cell types were considered as cell-type specific GOs (**Fig. 3E, 3F, and Fig. S20A**).

### Aging clock analysis

For aging clock analysis, we focused on 64 head and body cell types that have at least 200 cells at each time point. For each cell type satisfying the condition, we then built aging clock models – regression models that predict age from the transcriptome. In particular, for each cell type we trained the elastic net model (33) by using cells' transcriptome as explanatory (independent) variables and age as the response (dependent) variable. We randomly split the dataset into a train and test dataset where we used 70% of cells to train the model, and 30% of cells to validate the model. We compared the predictions to the true age and measured performance of the model as  $R^2$ , *i.e.*, proportion of the variance for a dependent variable that's explained by an independent variable or variables. We repeated the analysis over five random seeds, resulting in different train and test data splits. To find genes that correlate with age, we first filtered all genes with zero coefficient in the regression model. For the remaining genes, we calculated the Pearson correlation between its value and age and retained those genes for which the correlation coefficient was higher than 0.3. This analysis resulted in 480 genes. We repeated the same analysis for the Mouse Aging Cell Atlas (Tabula Muris Senis) (27).

To compare models between two consecutive stages, we trained three logistic regression models for each cell type to distinguish between (i) 5 days and 30 days old fly, (ii) 30 days and 50 days old fly, and (iii) 50 days and 70 days old fly. We split the data into train and test dataset by using 70% data for training the model and 30% data for evaluation by preserving the percentage of samples for each class (stratified sampling). We evaluated classification performance using accuracy.

### Identification of possible transcription factor(s) regulating the RP genes

Head and body regulons identified by SCENIC were obtained from FCA (7, 36). TF regulons containing more than 5 RP genes were considered to be the potential transcription factors. RP genes were removed from the regulon of each transcription factor and the average expression of RP and regulon genes was calculated in each cell type. The average expression of RP and regulon genes was clustered to find regulons showing gene expressions similar to the RP genes.

### Cell-identity analysis

Change in cell identity was based on the expression changes of marker genes between different ages. Cell-type markers from young (5d) and old animals (50d) were identified separately using the Wilcoxon Rank Sum test (`rank_genes_groups()` in SCANPY). The top 200 genes that are differentially expressed between cell types were defined as marker genes for each cell type. Expression of marker genes was further compared between young and old populations using the Wilcoxon Rank Sum test to identify differentially expressed markers ( $FDR < 0.05$ ). Young marker genes with a significant reduction of expression would be considered to decrease the cell-type

identity. On the other hand, old marker genes with a significant increase in expression were also considered to decrease the identity. Together, we used the average of these two ratios to indicate the change in cell identity.

## **AFCA website**

The AFCA Website was developed with the Shiny package (v1.6.0) in R language (v4.0.5). We included three major datasets: Head dataset, Body dataset, and Head and Body dataset, where they contain the snRNA-Seq analytical results from head tissues, body tissues, and combined respectively. For the Cell type and Gene Expression tabs, the data processing and visualization were performed with the Tidyverse (v1.3.0) and ggplot2 (v3.3.3) packages in R. For the customized analysis tab, its features and functions were powered by the ShinyCell (v2.1.0) package.

## **The rank sum of aging features**

We measured the absolute differences of each aging feature between the young (5d) and old (50d) population and ranked the cell-type differences. High ranks represented high aging differences, while low ranks indicated low differences between young and old populations. To have a better estimation, we focused on cell types with more than 200 nuclei from each age. Correlations of different aging features were compared using Spearman's correlation. To know which cell types showed high aging differences supported by different features, we summed the ranks of five different aging features and ranked the sums. High-rank sums of different aging features represented high aging differences and vice versa.

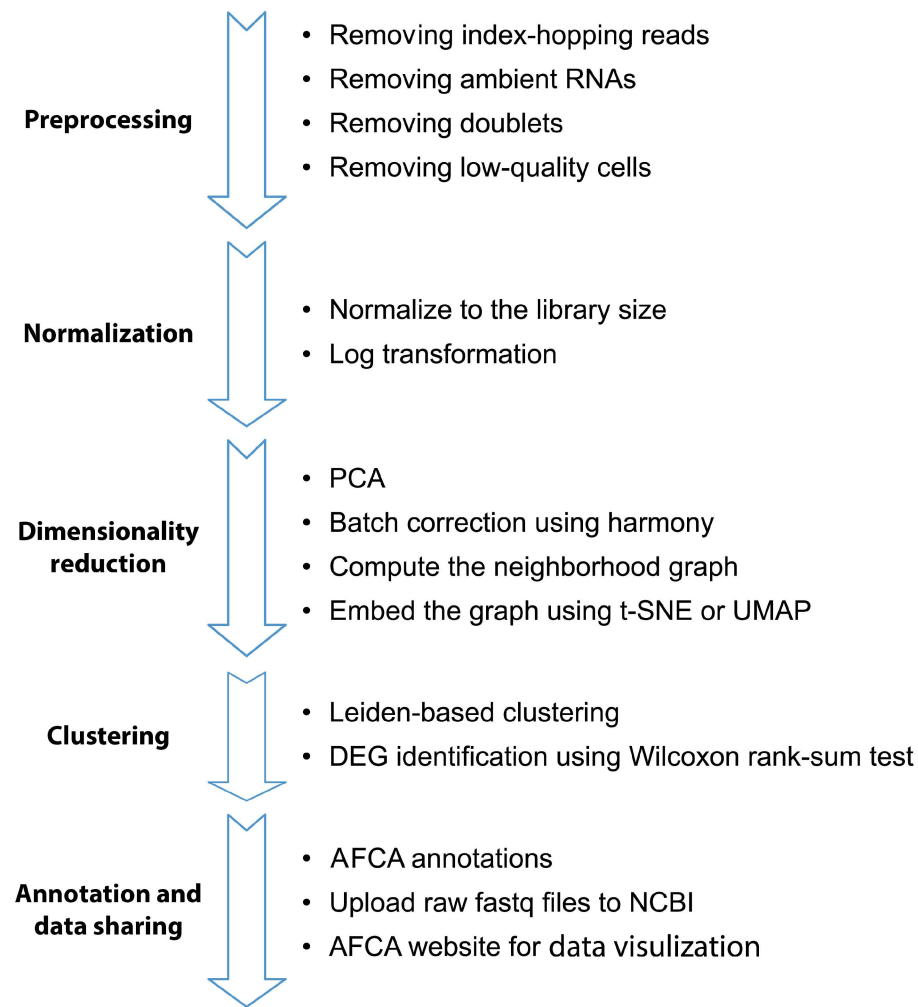
## **Analysis of alternative polyadenylation (APA) analysis**

Our overall analysis strategy was based on our recent scAPA study of the FCA dataset (50). We used LABRATsc (<https://github.com/TaliaferroLab/LABRAT>) to quantify APA from the scRNA-seq data with current FlyBase *Drosophila melanogaster* gene annotation (version r6.45). Two modes were used for either single-cell level (cellbycell) or cell-type specific (subsampleClusters) quantification using '--mode' parameter. We used read coverage thresholds of at least 3 or 100 counts per gene for single-cell level or cell-type specific quantification respectively to minimize noise and false positives. LABRAT calculates  $\psi$  values reflecting 3' isoform usage, with "0" indicating exclusive usage of the most proximal pA site, while "1" indicates exclusive usage of the most distal pA site.  $\Psi$  values for each annotated cell-type, and for individual cells, were used for downstream analysis.

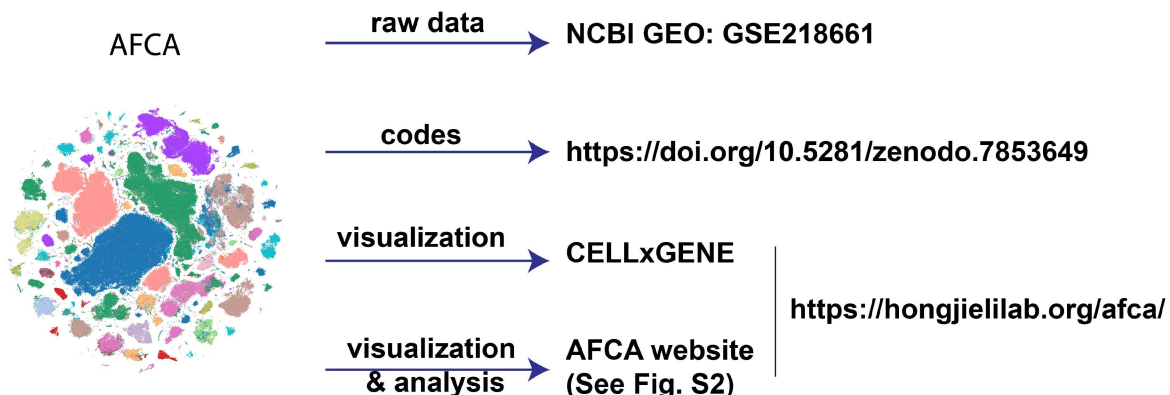
**Figs. S1 to S30**

Figure S1

## A data processing steps



## B data availability



**Fig. S1. General pipeline of snRNA-seq analysis and data availability.**

A) Data processing steps, including preprocessing, normalization, dimensionality reduction, clustering, annotation, and data sharing. B) Data available from different sources, including NCBI, GitHub, CELLxGENE, and AFCA website.

# Figure S2

**Aging Fly Cell Atlas**

<https://hongjielilab.org/afca/>

The interface includes a top navigation bar with links for AFCA, Home, Head Dataset, Body Dataset, Head and Body Dataset, and Downloads.

**cell type-based analysis**

- cell type from 4 ages
- marker genes
- aging features
  - a. change of cellular composition
  - b. # DEG
  - c. # gene & UMI
- age-related genes

**gene-based analysis**

- expression in all cell types
- expression in one cell type
- ranking cell types by changes

**custom analysis**

- gene co-expression
- compare cell types
- compare genes
- multi-gene plot

**Fig. S2. AFCA web portal for surveying the age-related changes.**

AFCA web portal provides cell type-based, gene-based, and customized analysis.

# Figure S3

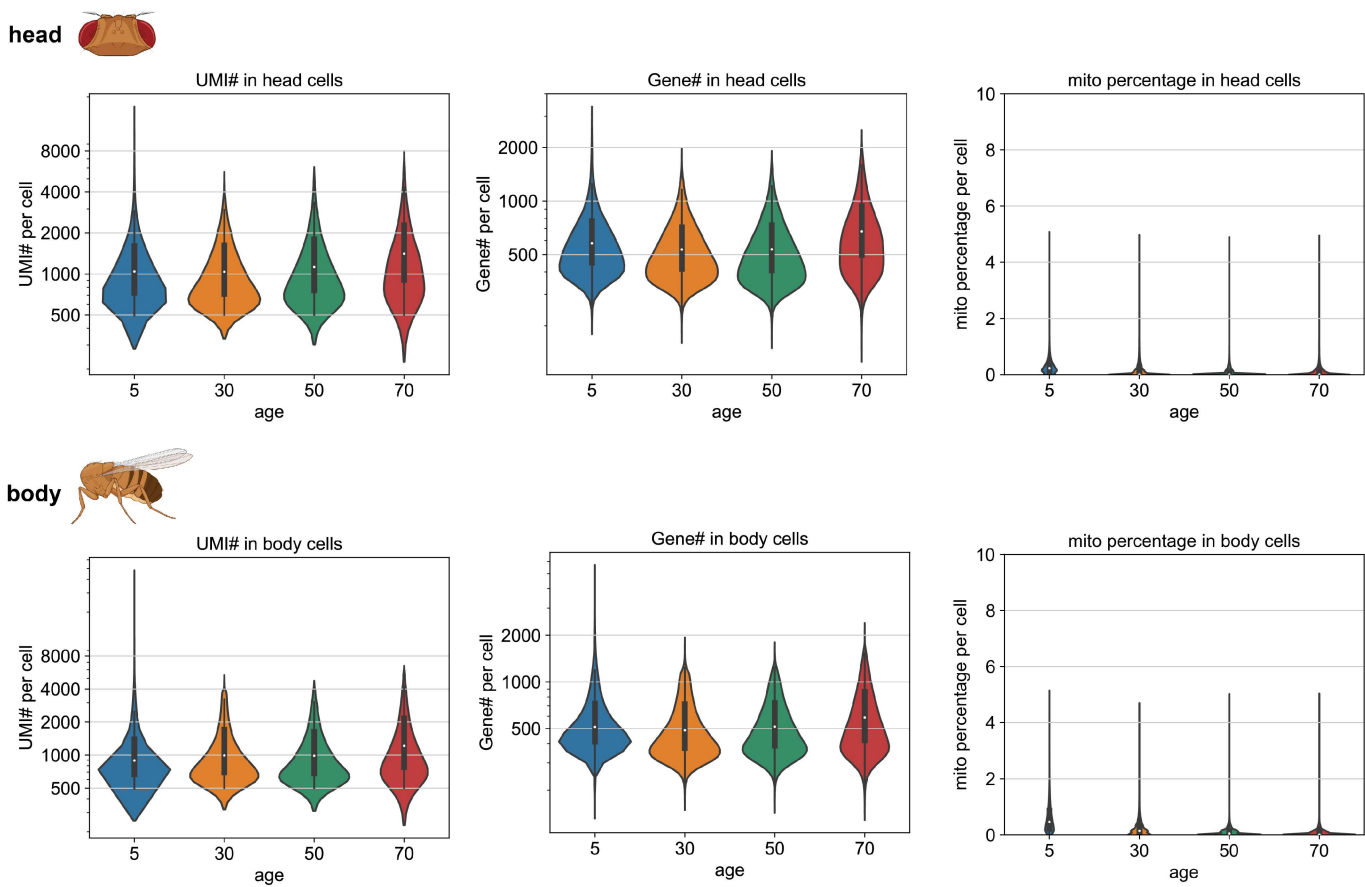


**Fig. S3. General quality of snRNA-seq results.**

UMI number, expressed gene number, and mitochondria transcript ratio from the AFCA data.

# Figure S4

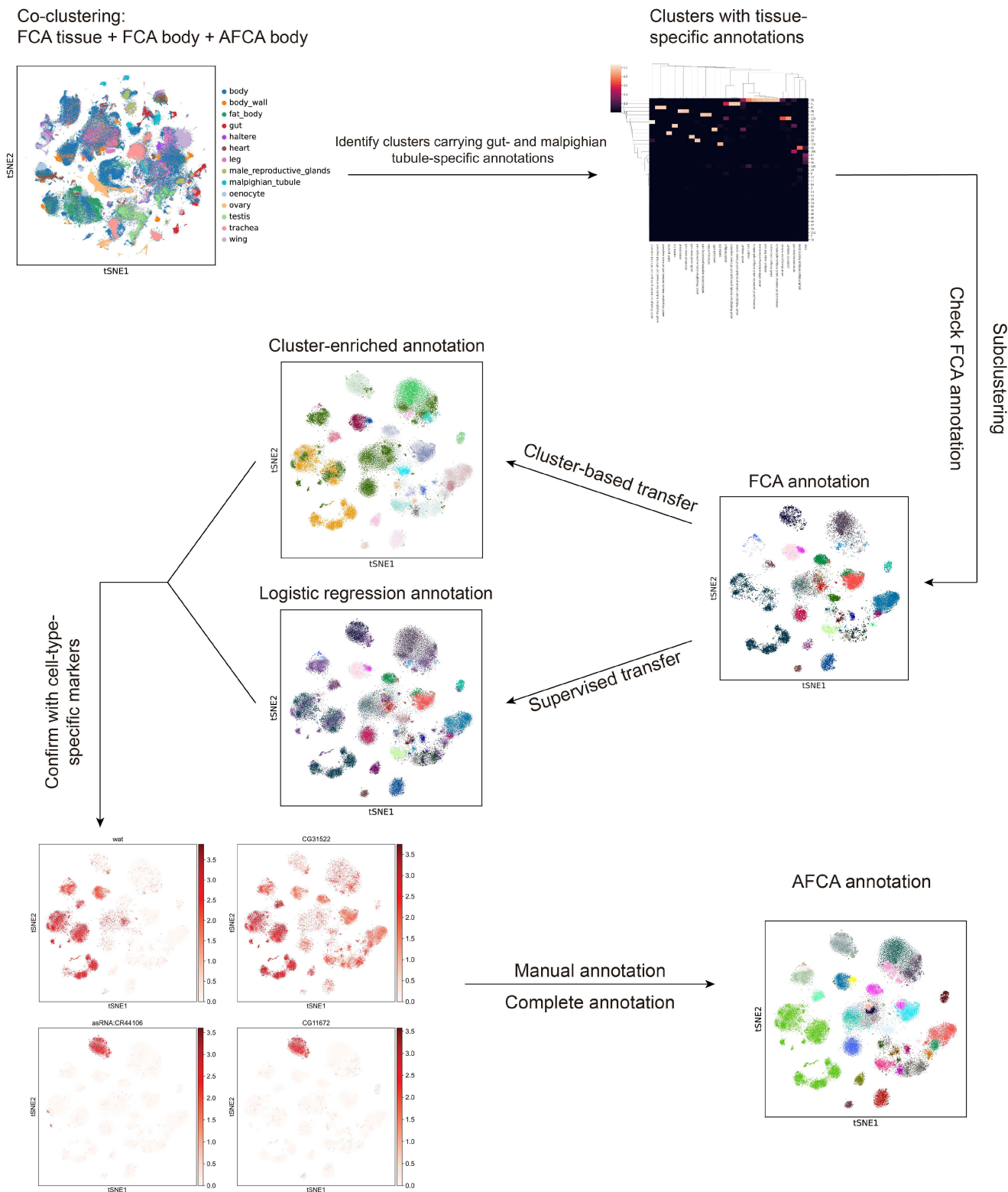


**Fig. S4. Illustration of transferring the FCA annotation to the AFCA cells.**

Flowchart of transferring the annotations from FCA to AFCA. FCA and AFCA data are first co-clustered. Co-clustered data can be further extracted for tissue-specific cell types, e.g. gut- and malpighian tubule-specific cell types. After subclustering targeted cells, FCA annotations are transferred to AFCA cells using cluster-based or supervised machine-learning approaches. Results from two transfer methods are compared and ambiguous transfers are further checked for the expression of the corresponding marker genes. After confirming the expression of the marker genes, annotations are corrected and finalized.

## Figure S5

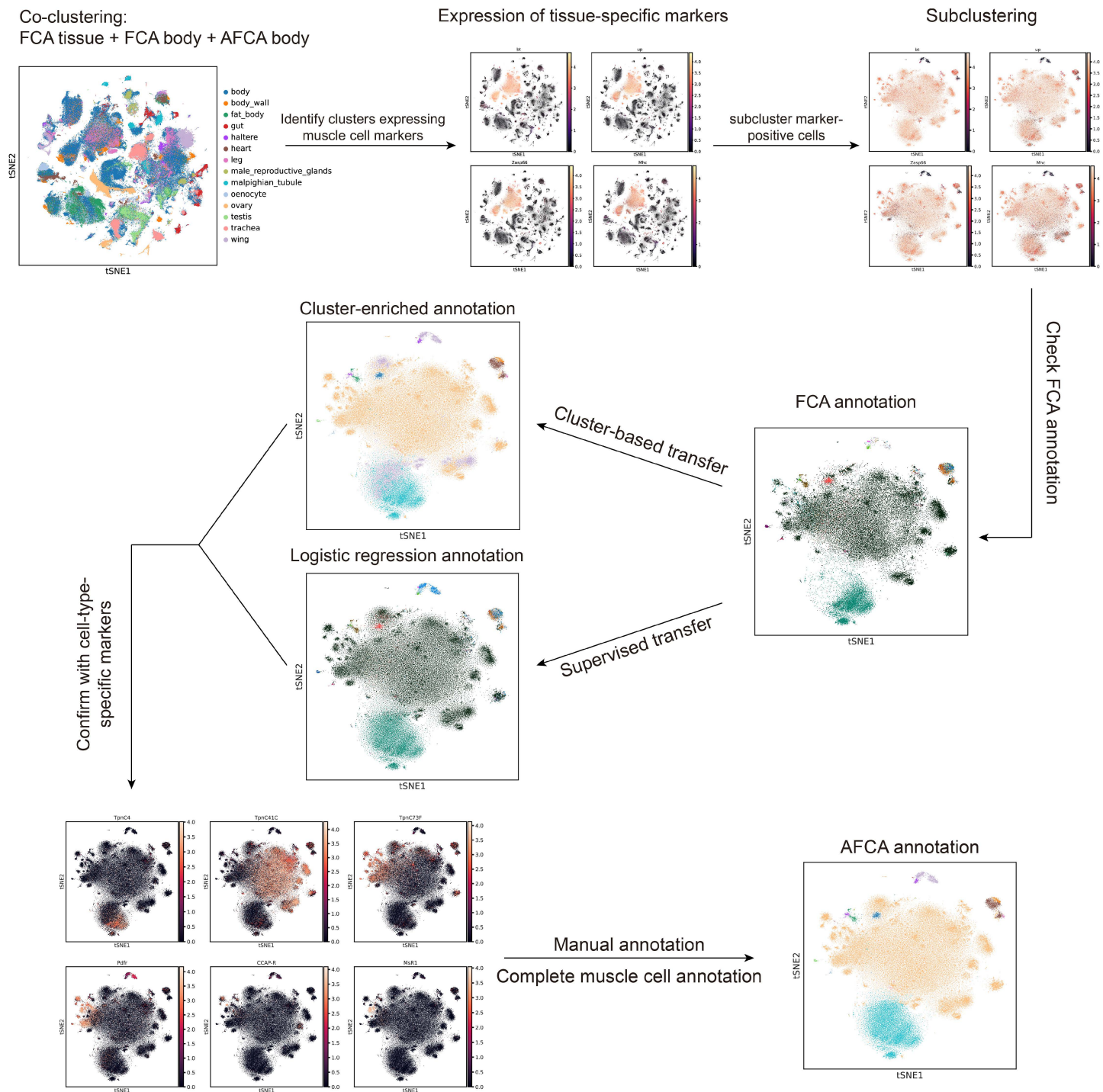


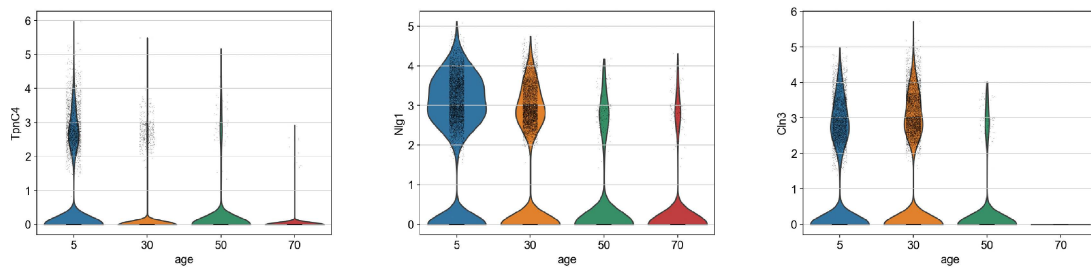
**Fig. S5. Illustration of transferring the FCA annotation to the AFCA muscle cells.**

Flowchart of transferring the muscle-type annotations from FCA to AFCA. Some cell types, like muscle cells, can be found in multiple tissues and we consider first extracting those cells based on the expression of general markers of muscle cells. After subclustering the corresponding cells, all remaining analyses are similar to approaches used in **Fig. S4**.

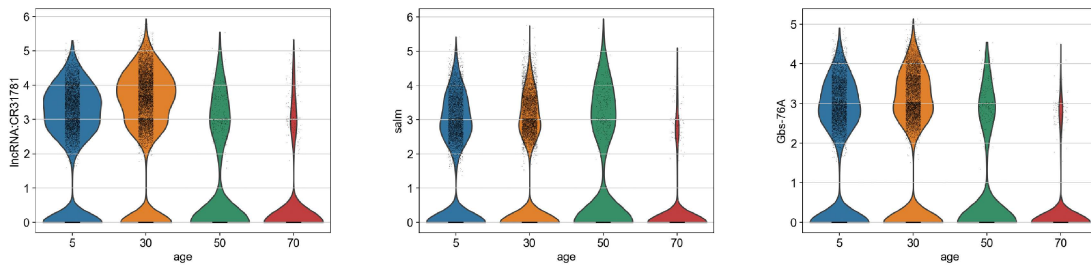
# Figure S6

A

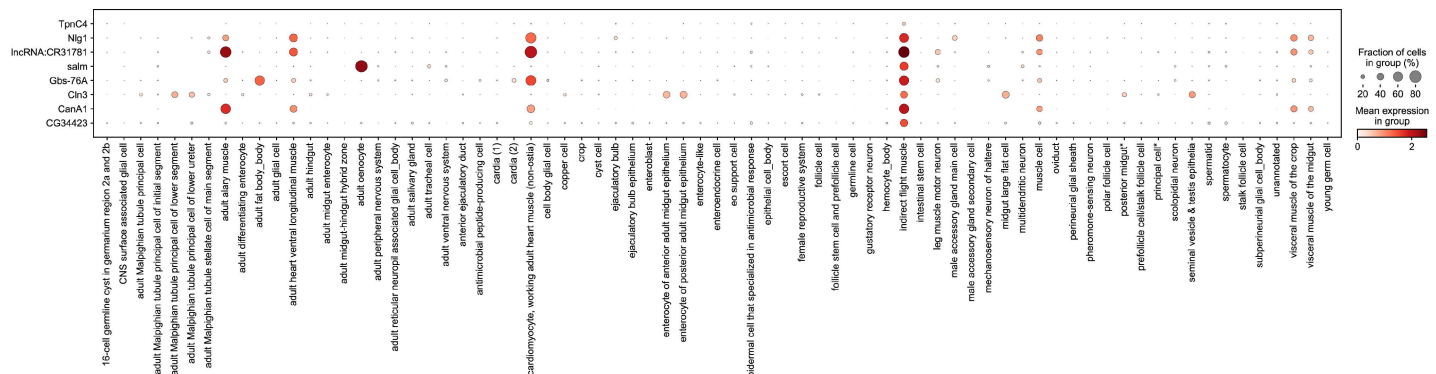
## Decreased expression of marker genes from the indirect flight muscle



## Other marker genes from the indirect flight muscle



B Marker genes from the indirect flight muscle



C Overlapped marker genes from two stem cells

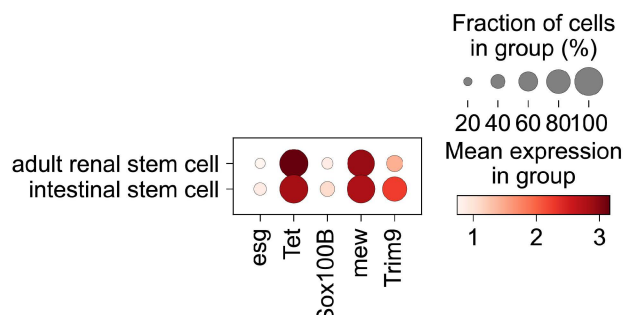


**Fig. S6. Ambiguous annotations from the aging samples.**

A, B) Marker genes of the indirect flight muscle. A) Loss of marker genes in the indirect flight muscle. B) Markers specific for the indirect flight muscle. C) Overlapped marker genes from renal stem cells and intestinal stem cells.

# Figure S7

Gut & Mal. tubule cells

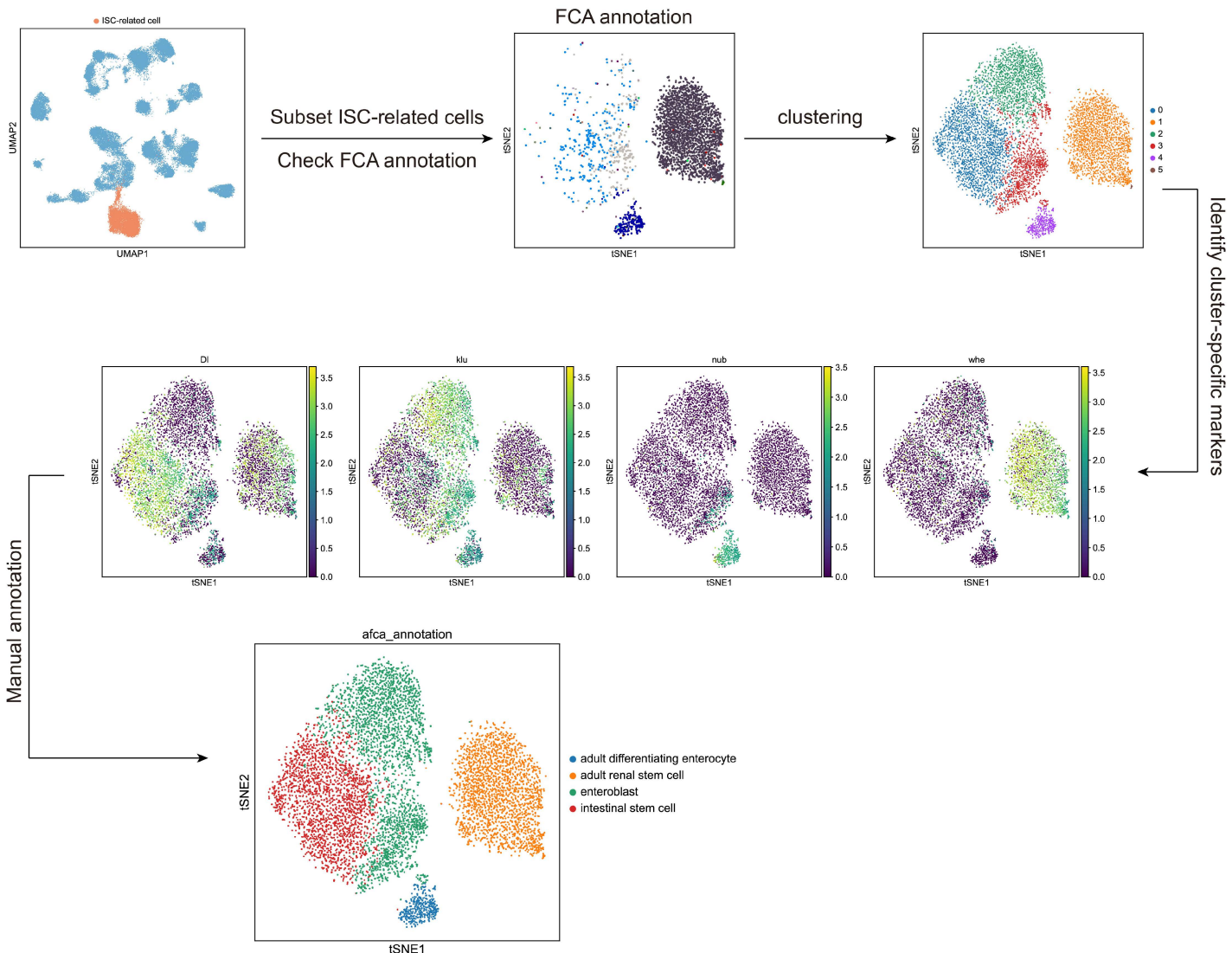


**Fig. S7. Illustration of manually annotating ISCs, EBs, and renal stem cells.**

Flowchart of manual annotation of the stem cell population. ISCs, EBs, and differentiating enterocyte cells are selected from the gut and malpighian tubule dataset shown in **Fig. S4**. Marker genes enriched in each cluster are identified and confirmed.

## Figure S8

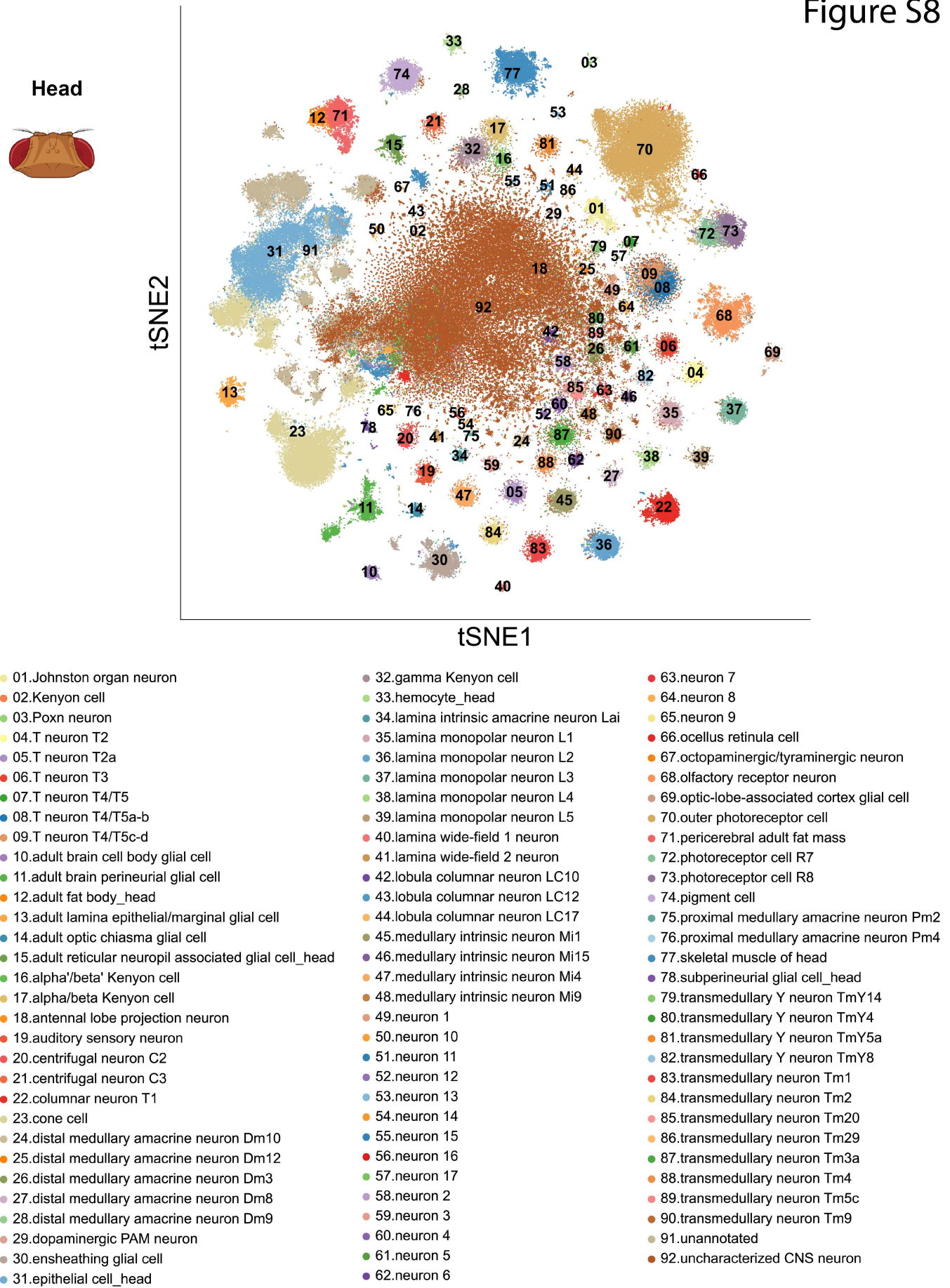


**Fig. S8. Detailed cell types annotated in the head sample shown by tSNE.**  
91 head cell types are shown in the tSNE plot.

# Figure S9

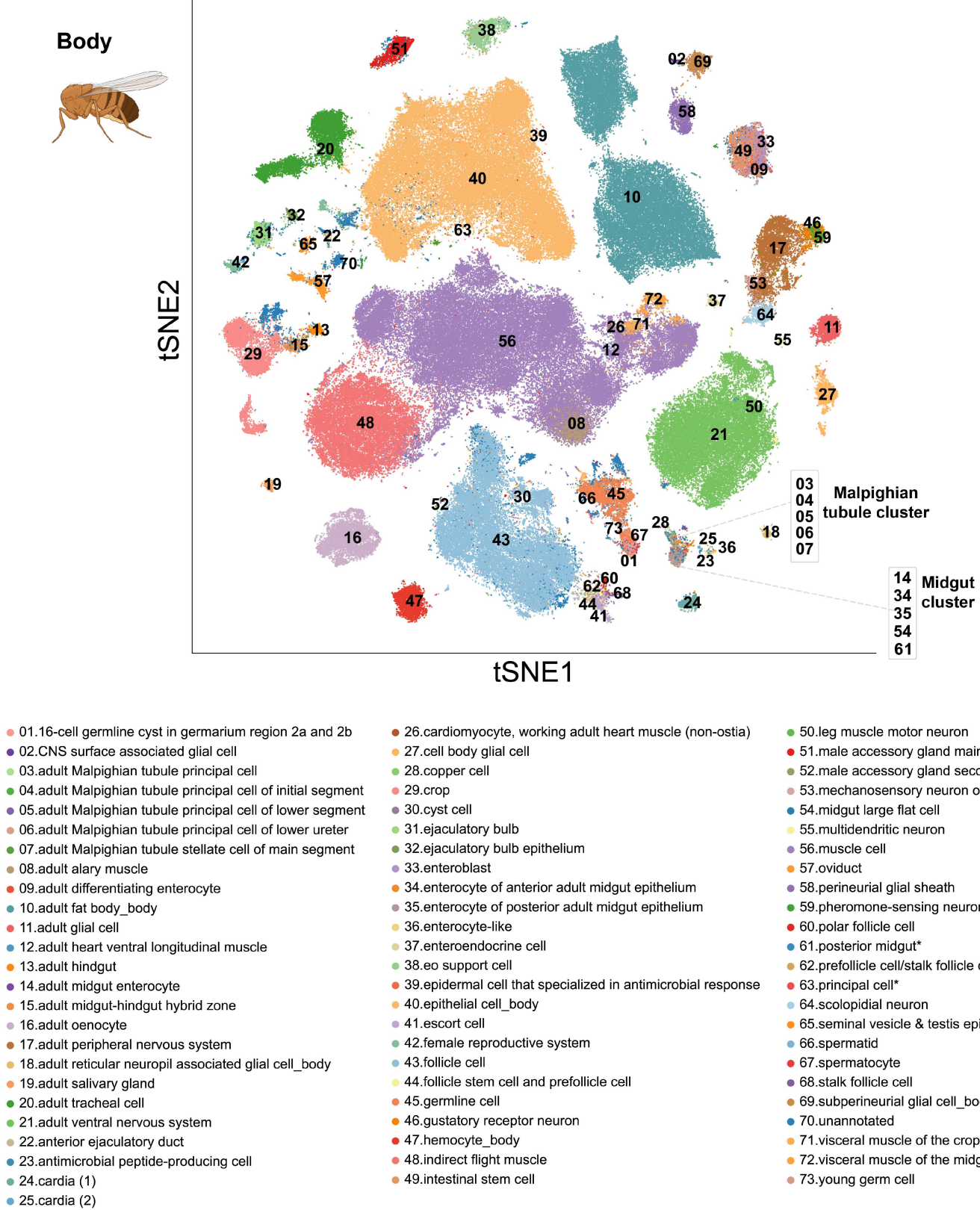


**Fig. S9. Detailed cell types annotated in the body sample shown by tSNE.**  
72 body cell types are shown in the tSNE plot.

## Figure S10

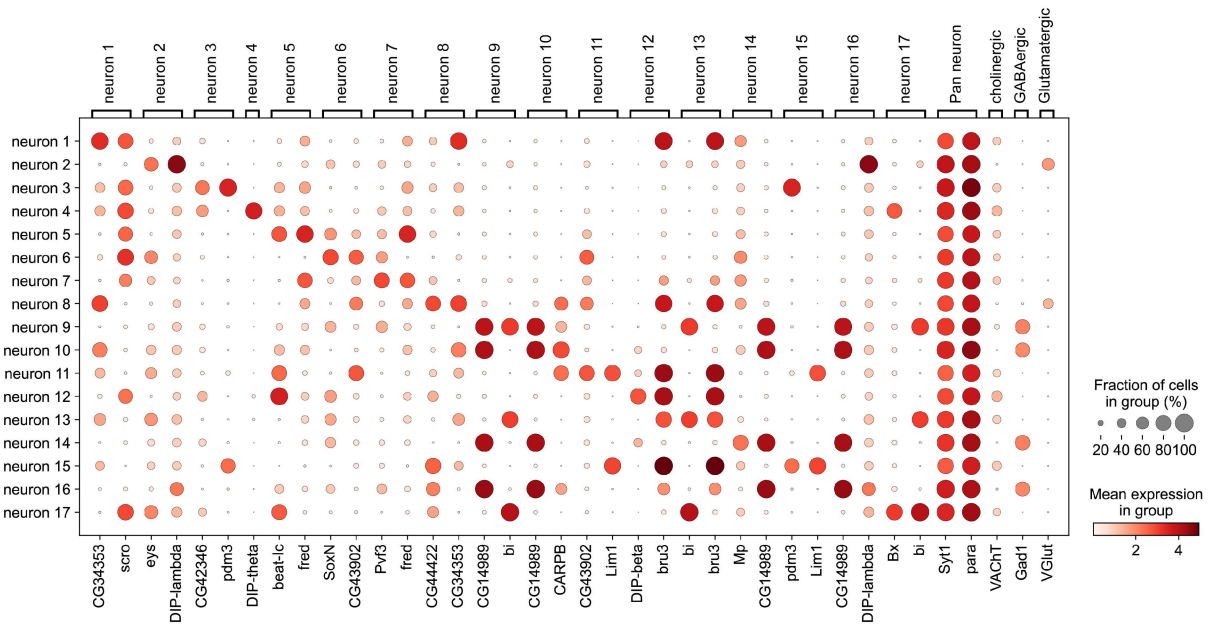


**Fig. S10. Marker genes identified from the newly identified neuron clusters.**

Markers of 17 newly identified neuron types are shown. Expression of general neuronal markers, Syt1, and para, indicates neuron specificity. Expression of VACChT, Gad1, and VGluT indicates they are cholinergic, GABAergic, or Glutamatergic neurons.

# Figure S11

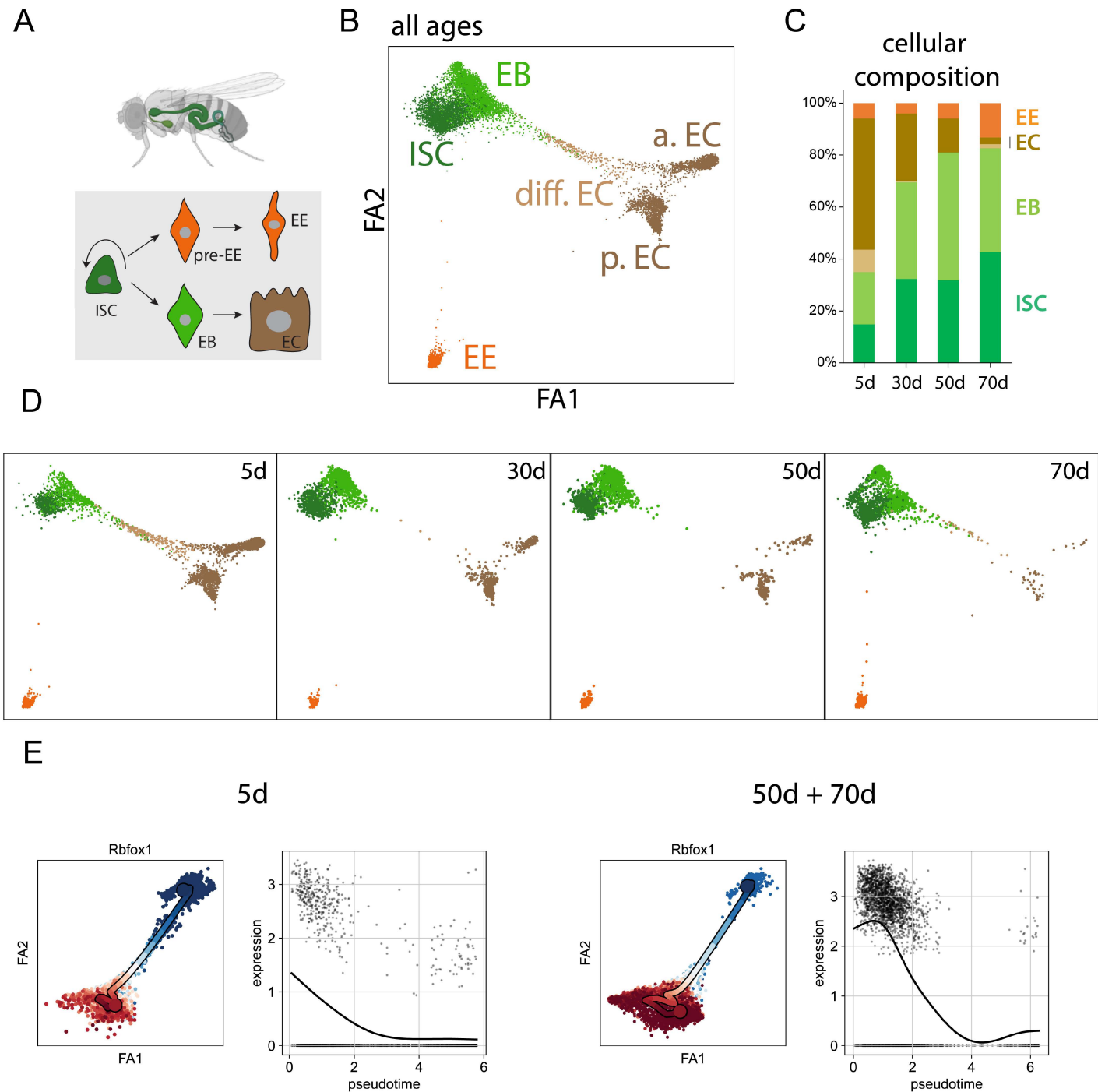
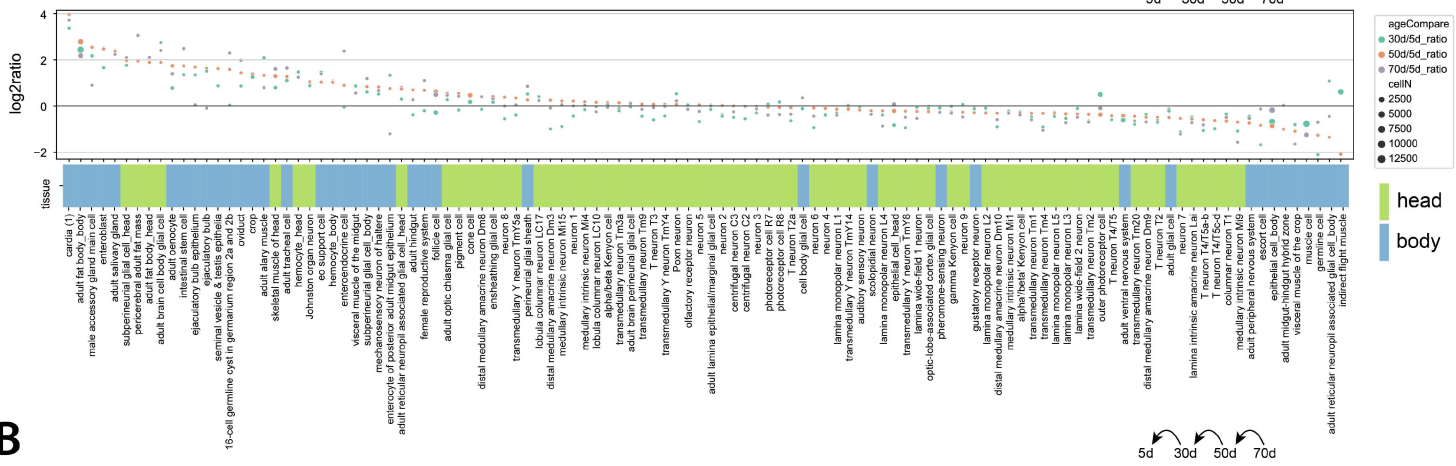


**Fig. S11 Pseudotime inference and cellular composition of ISC and ISC-differentiated cell types.**

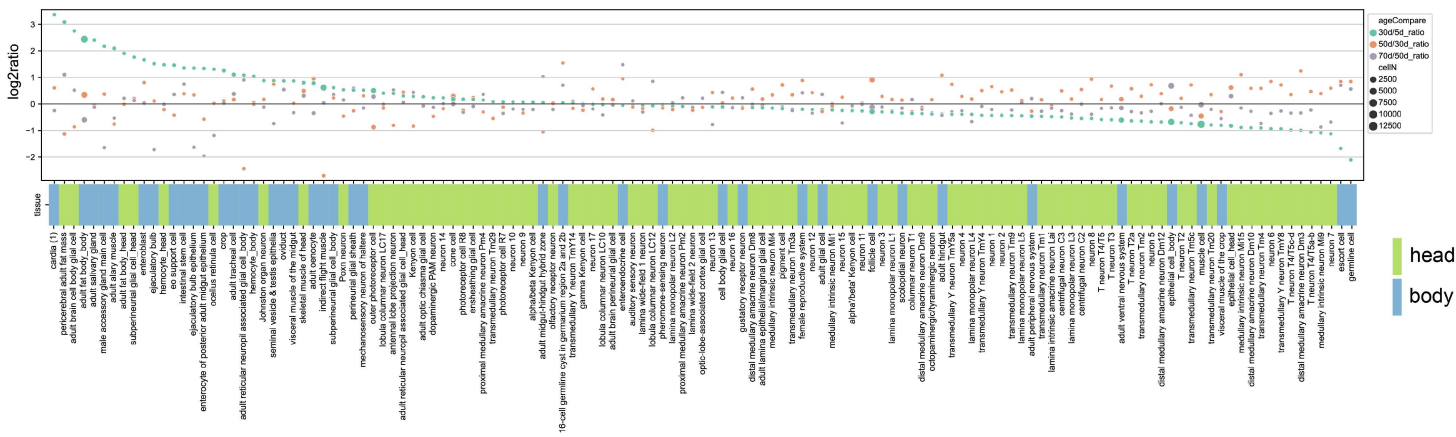
A) Illustration of ISC differentiation process. B) Cell types shown in different colors. C) Changes of cellular composition in the ISC lineage. D) Age-specific profile of different cell types. E) Rbfox1 gene shows different patterns along the young and old ISC lineage. ISC, intestinal stem cell; EB, enteroblast; EC, enterocyte; EE, enteroendocrine cell; a. EC, anterior EC; p. EC, posterior EC; diff. EC, differentiating EC.

# Figure S12

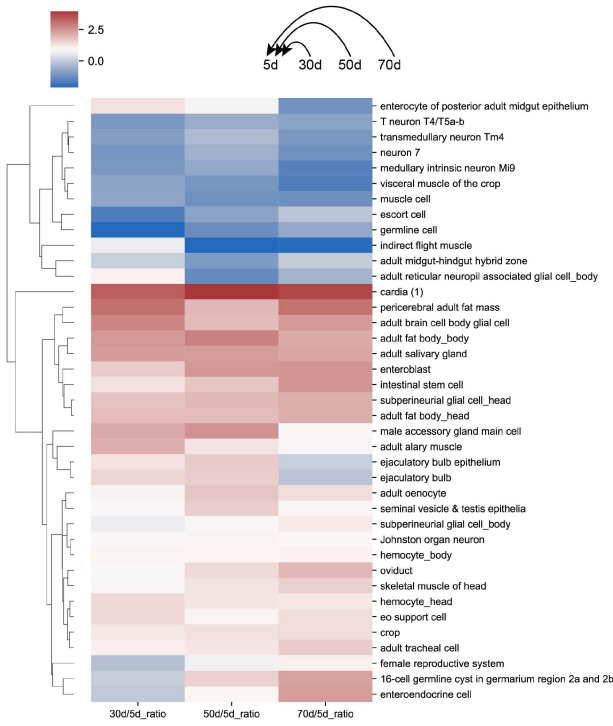
**A**



**B**



**C**



**D**

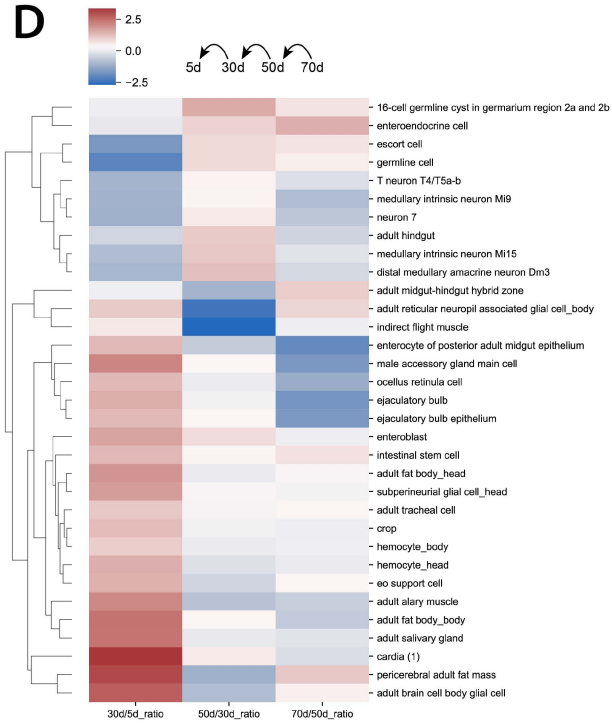
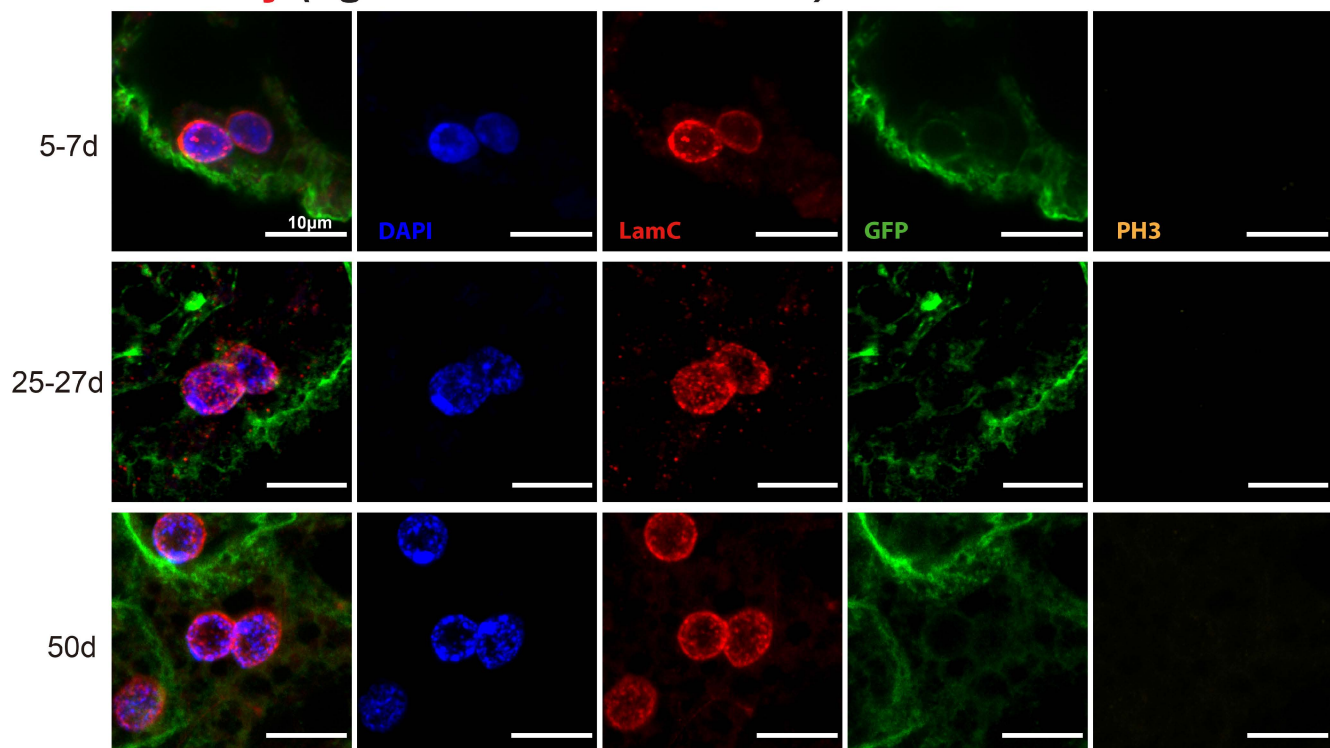


**Fig. S12 Changes of cell-type composition during aging.**

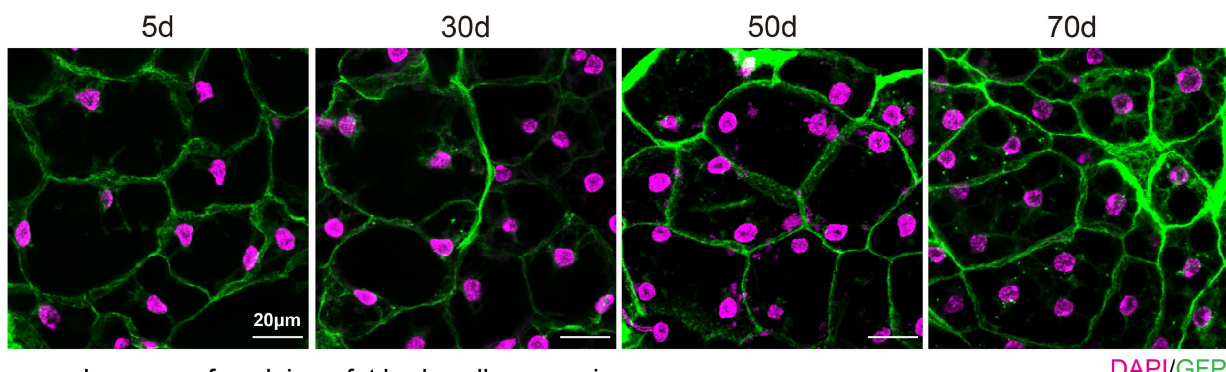
A) Changes in cellular composition by comparing the nuclear ratio of the old sample (30d, 50d, and 70d) to the ratio of the young one (5d). B) Changes of cellular composition by comparing the nuclear ratio between two consecutive ages. C) Cell types with more than 2-fold changes of cellular composition by comparing the old samples to the young ones. D) Cell types with more than 2-fold changes of cellular composition by comparing the sample to the previous age.

Figure S13

**A fat body (*cg-GAL4>UAS-CD8GFP*)**



**B**



Increase of nuclei per fat body cell upon aging

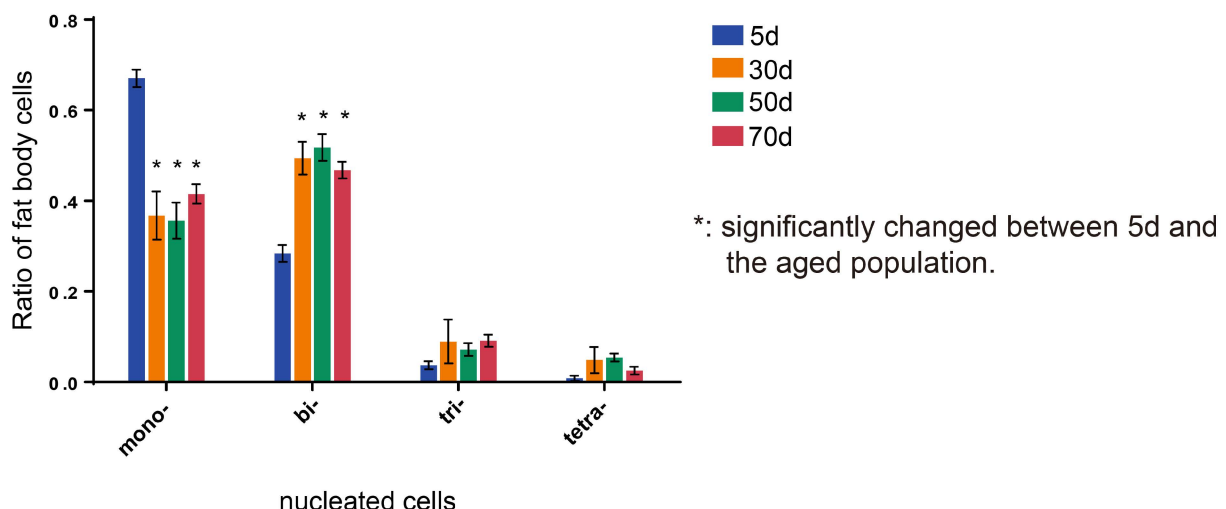
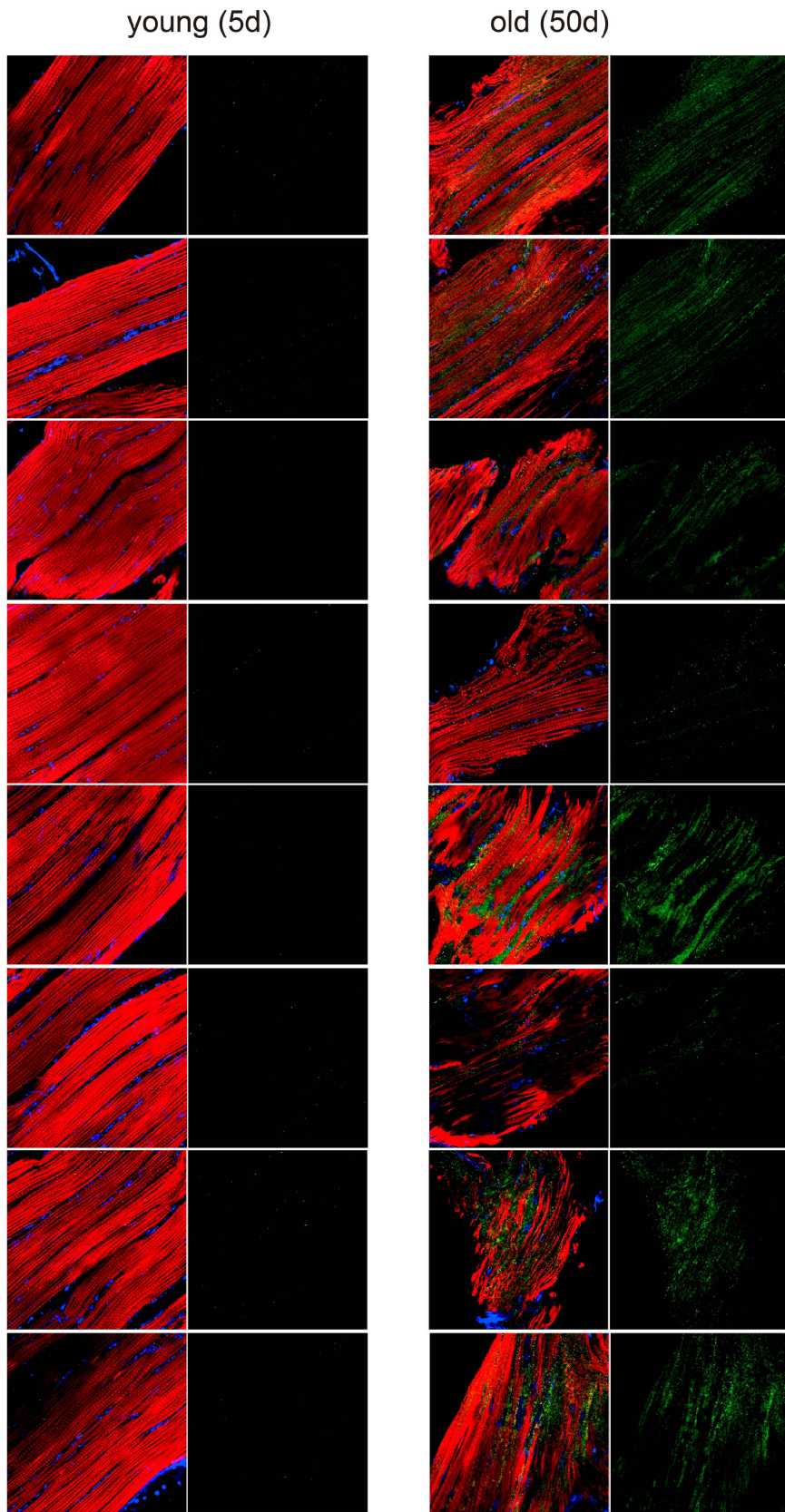


**Fig. S13. Examples of dividing nuclei without the mitosis marker.**

A) Dividing nuclei from flies with different ages showing the absence of the mitosis marker (pH3). Fat body nuclei are collected from different ages, including 5-7d, 25-27d, and 50d. Dividing nuclei are stained by DAPI and LamC. The fat body membranes are labeled by *cg-GAL4 > UAS-CD8GFP*. B) The multinucleation of fat body cells in aged flies. The representative images of fat bodies of different ages are shown. The multinucleation of the fat body was examined for at least 324 cells (5d:359, 30d:324, 50d:369, and 70d:494 cells) in 7-10 animals of each age. The two-way ANOVA and Tukey's multiple comparisons test were performed. The asterisks show the P<0.0001.

Figure S14

indirect flight muscle



DAPI/Phalloidin/Caspase3

**Fig. S14 Apoptosis signals form the aged indirect flight muscle.**

Examples of indirect flight muscle stained by the apoptosis marker in the young and old flies. The indirect flight muscles are stained for the apoptosis events using a cleaved-Caspase3 antibody. Nuclei are stained by DAPI. Actin filaments in the muscle cells are labeled by Phalloidin.

# Figure S15

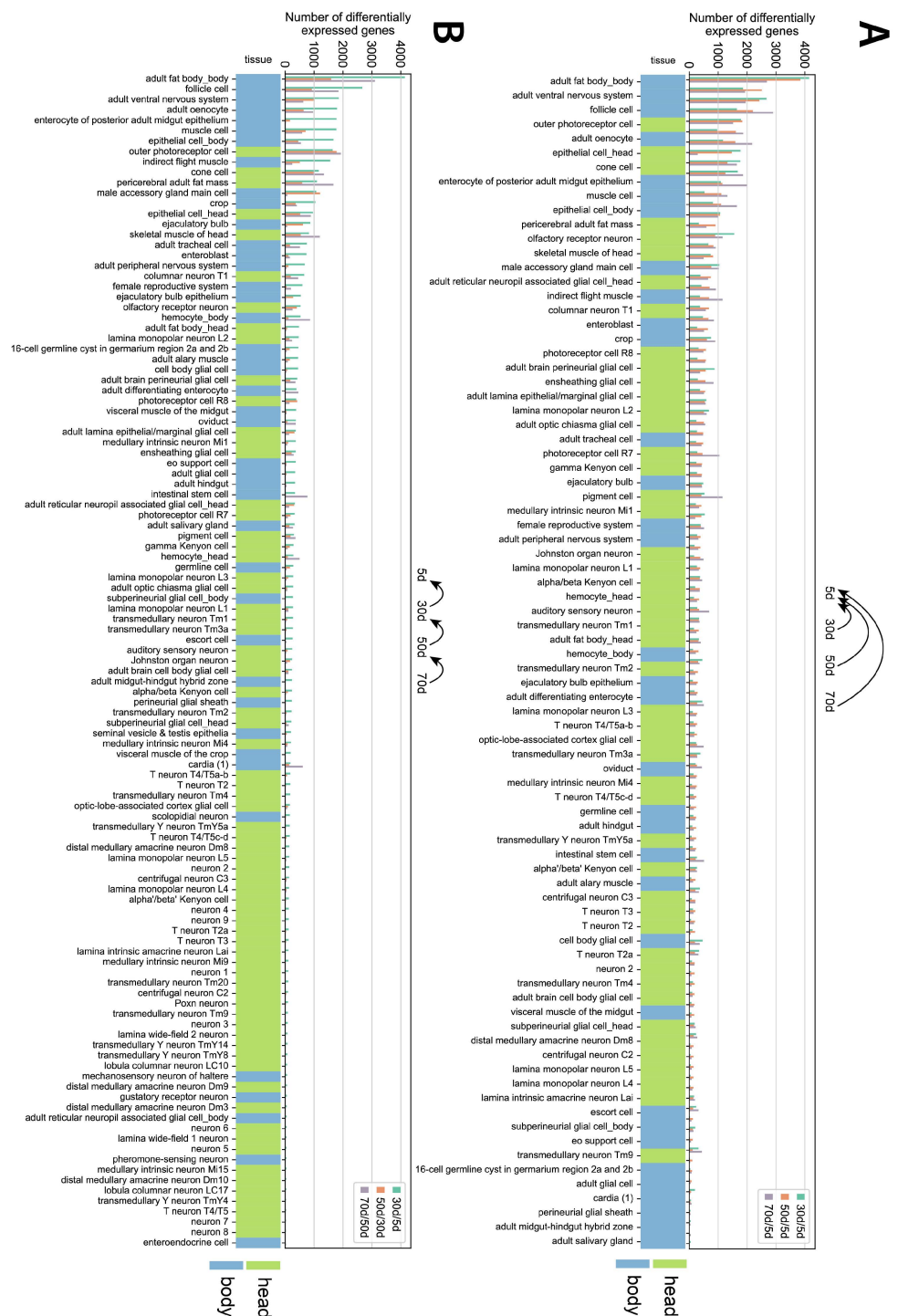


**Fig. S15 DEG numbers detected in each cell type.**

A) DEG numbers from different cell types. The aged groups (30d, 50d, and 70d) are compared with the young population (5d). B) Two consecutive ages are compared to identify DEGs in each cell type.

# Figure S16

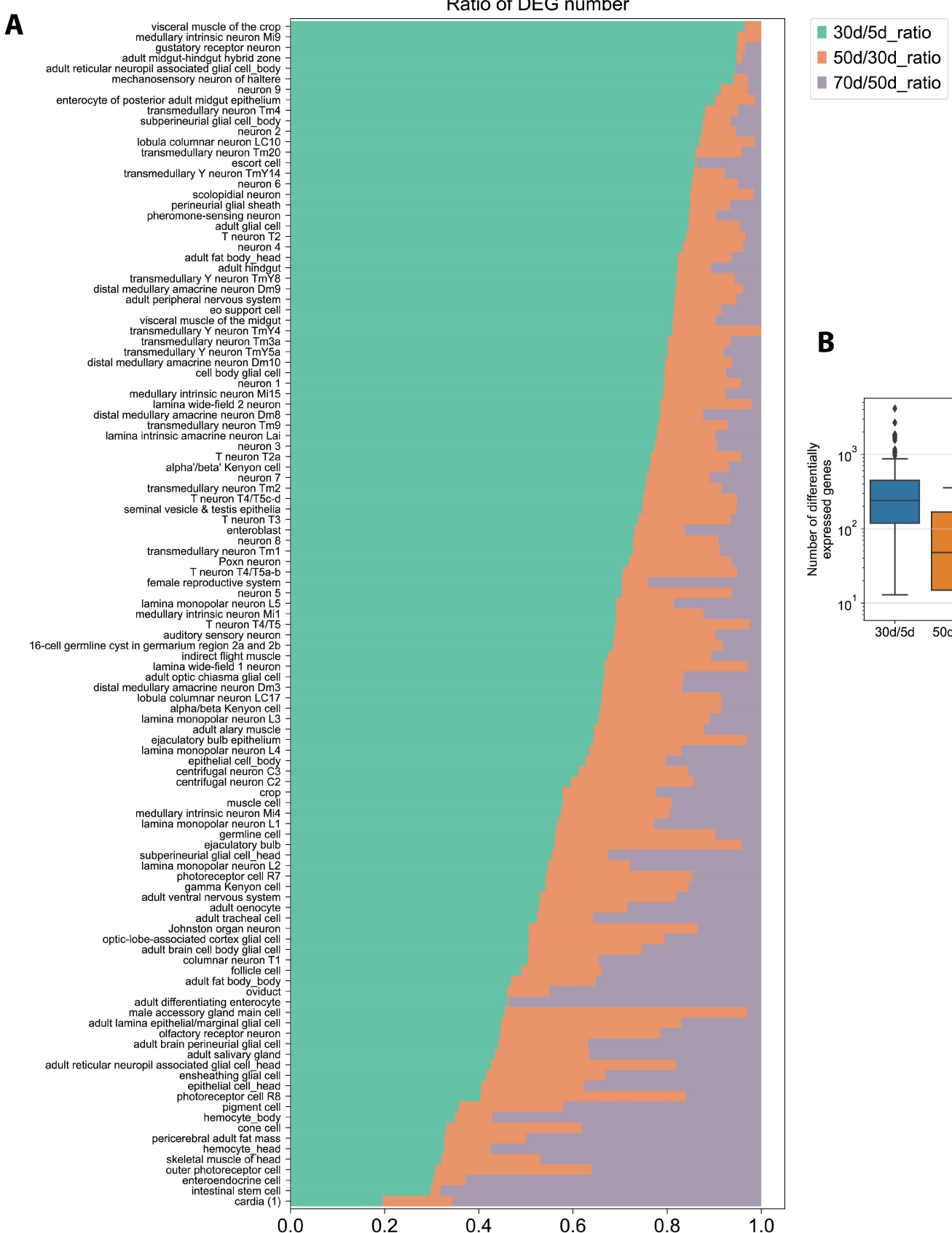
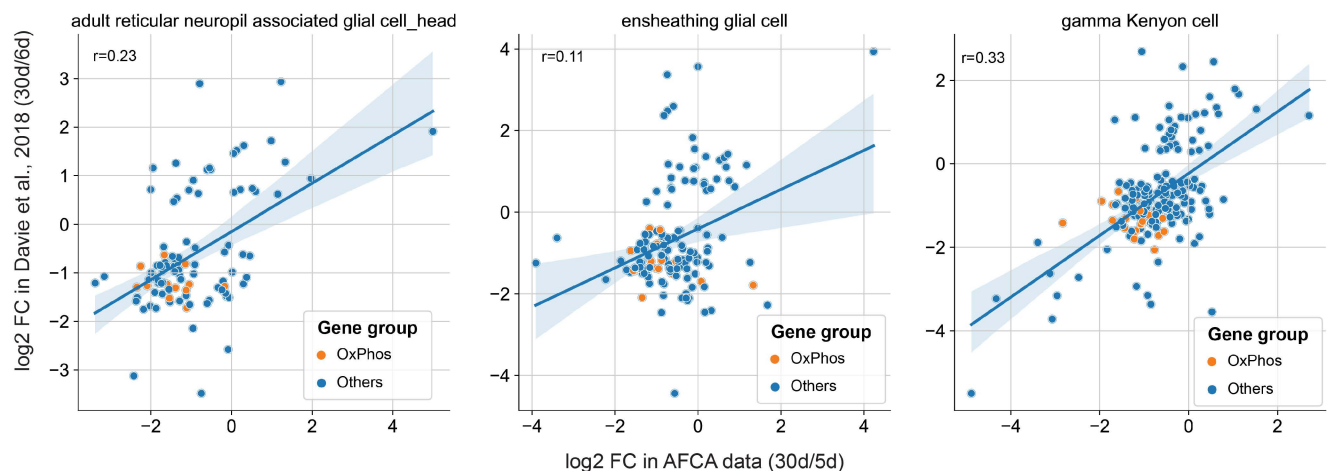


**Fig. S16 Detailed ratio of DEG number across different age periods.**

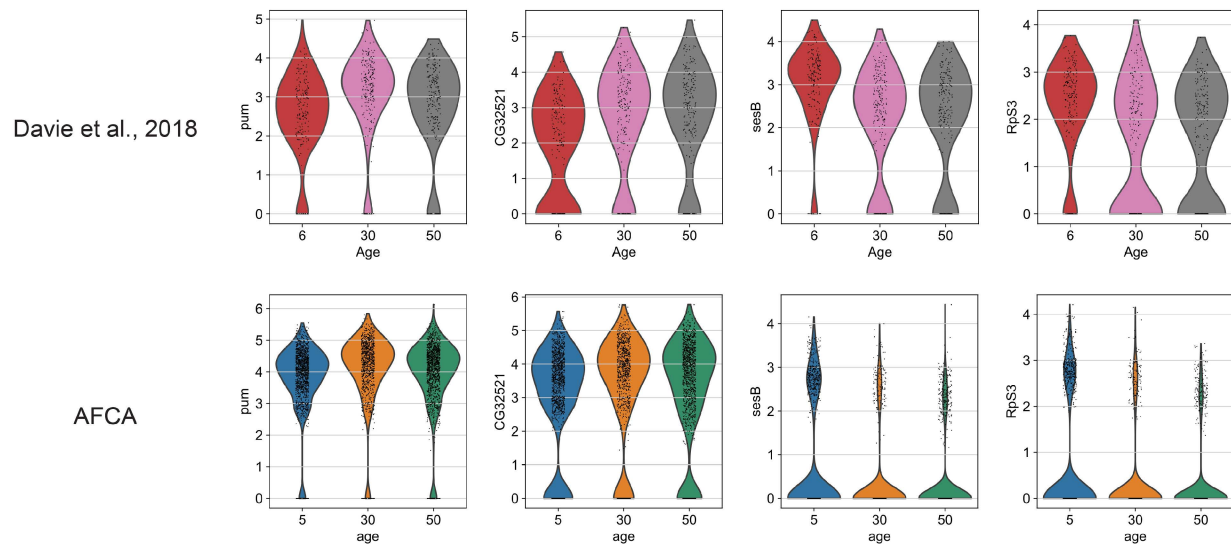
- A) The ratios of DEG numbers in different cell types. Each age period is shown in a different color.
- B) Number of differentially expressed genes detected in the different age periods.

# Figure S17

## A DEG comparisons between AFCA and Davie et al., 2018



## B ensheathing glial cell



## C DEG ratio in Davie et al., 2018

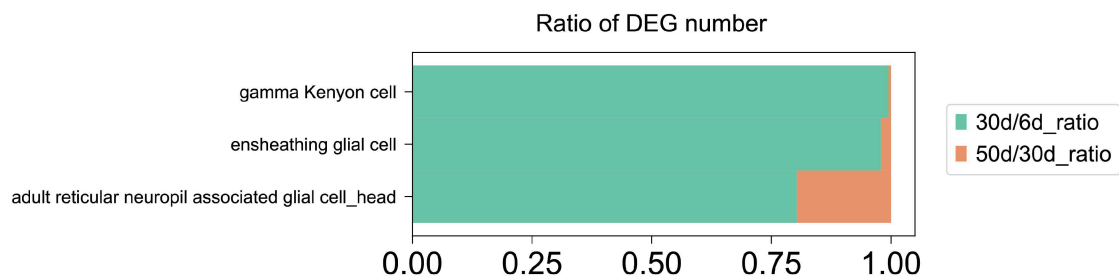


**Fig. S17. Comparisons between AFCA and Davie et al., 2018 data.**

A) Three cell types with the highest cell number from Davie et al., 2018 are compared to the corresponding cell types in the AFCA. X-axis indicates the log2 fold changes of gene expression between 30d and 5d samples in AFCA, while Y-axis represents the log2 changes between 30d and 6d samples in Davie et al., 2018. Orange dots are genes related to oxidative phosphorylation. Pearson correlations are performed to measure the correlation of log2 fold changes between two datasets. B) Aging DEGs in ensheathing glial cells are similarly regulated in AFCA and Davie et al. 2018 samples. C) Three cell types show a higher DEG ratio in the 30d/6d age interval compared to the 50d/30d one.

# Figure S18

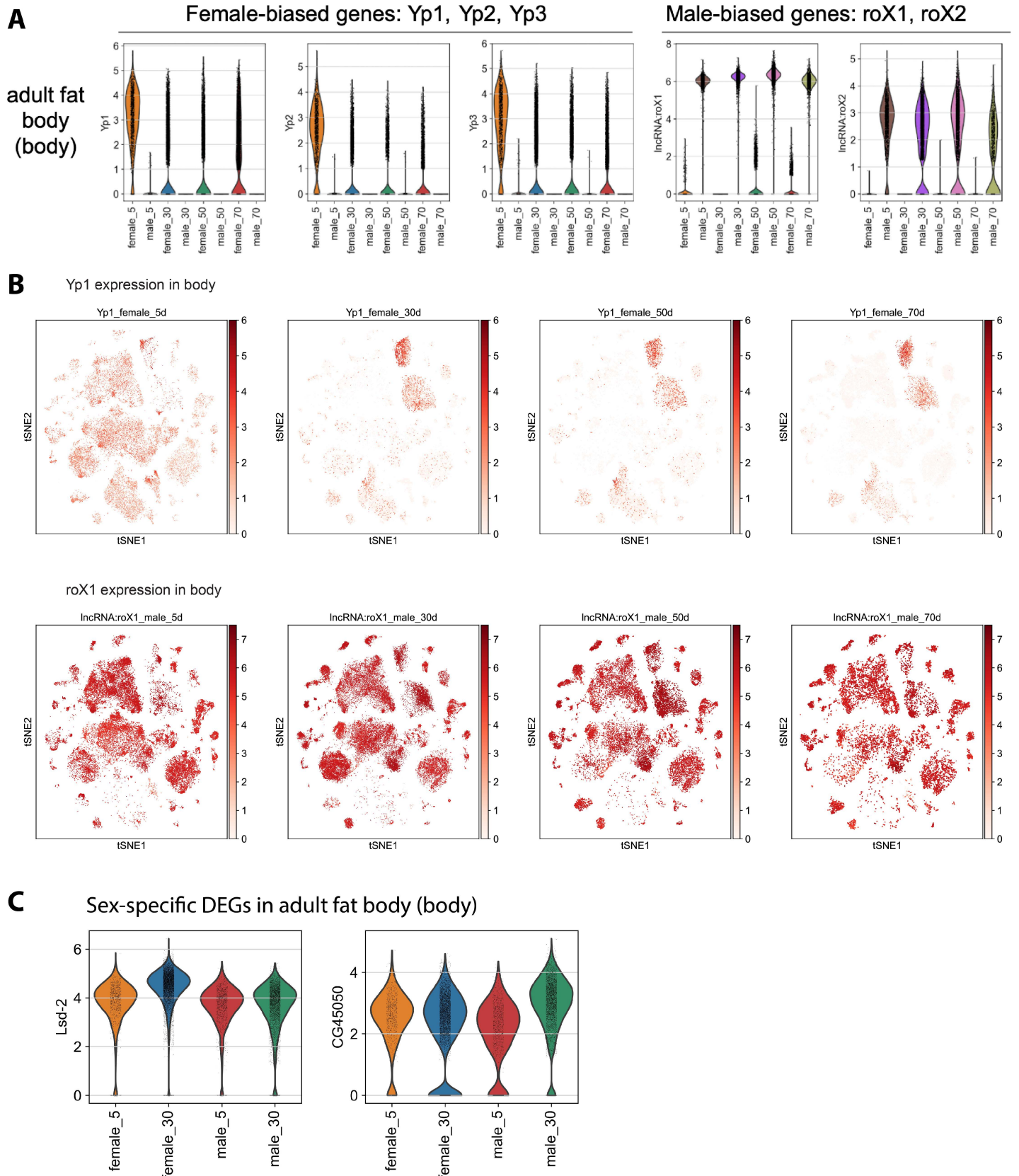


**Fig. S18 Sex-specific expression of genes.**

A) Expression of female- and male-biased genes from the fat body cells during aging. B) Expression of *Yp1* and *roX1* in body cells shown by tSNE. C) two example genes showing different change trends between males and females.

# Figure S19

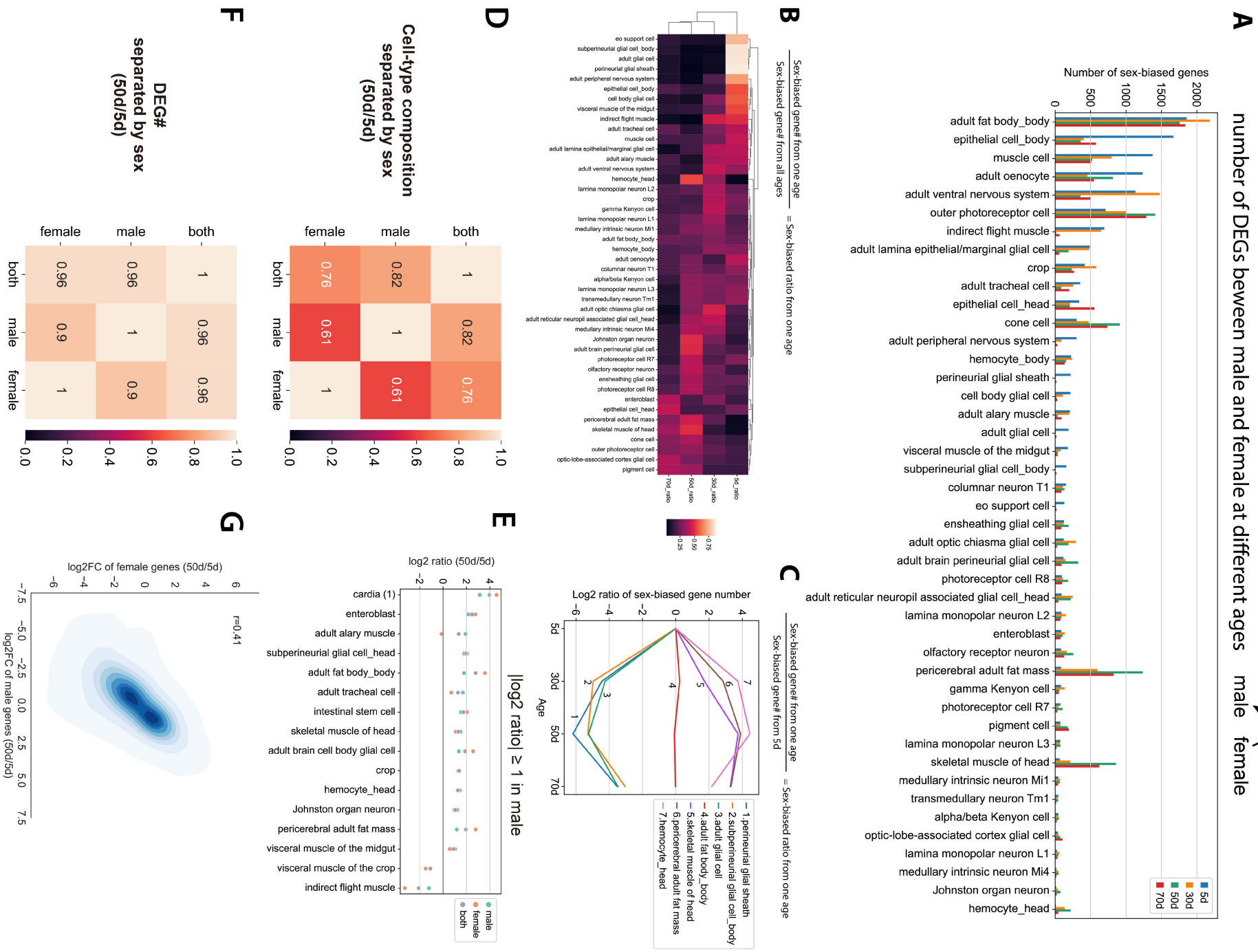


**Fig. S19 Sex-biased genes from each age.**

A) The number of sex-specific genes from each age. B) Sex-biased ratios from different ages. C) Illustration of sex-biased ratios from several cell types. D) Spearman's rank correlation of the change of cell-type composition between males and females. (E) Log2 ratio of cell-type composition by comparing 50d to 5d samples in different sexes of flies. (F) Spearman's rank correlation of DEG number from each cell type by comparing 50d to 5d samples in male or female flies. (G) Comparison of log2 fold changes of gene expression between male and female. The Pearson correlation coefficient of male and female log2 fold changes is 0.41.

## Figure S20

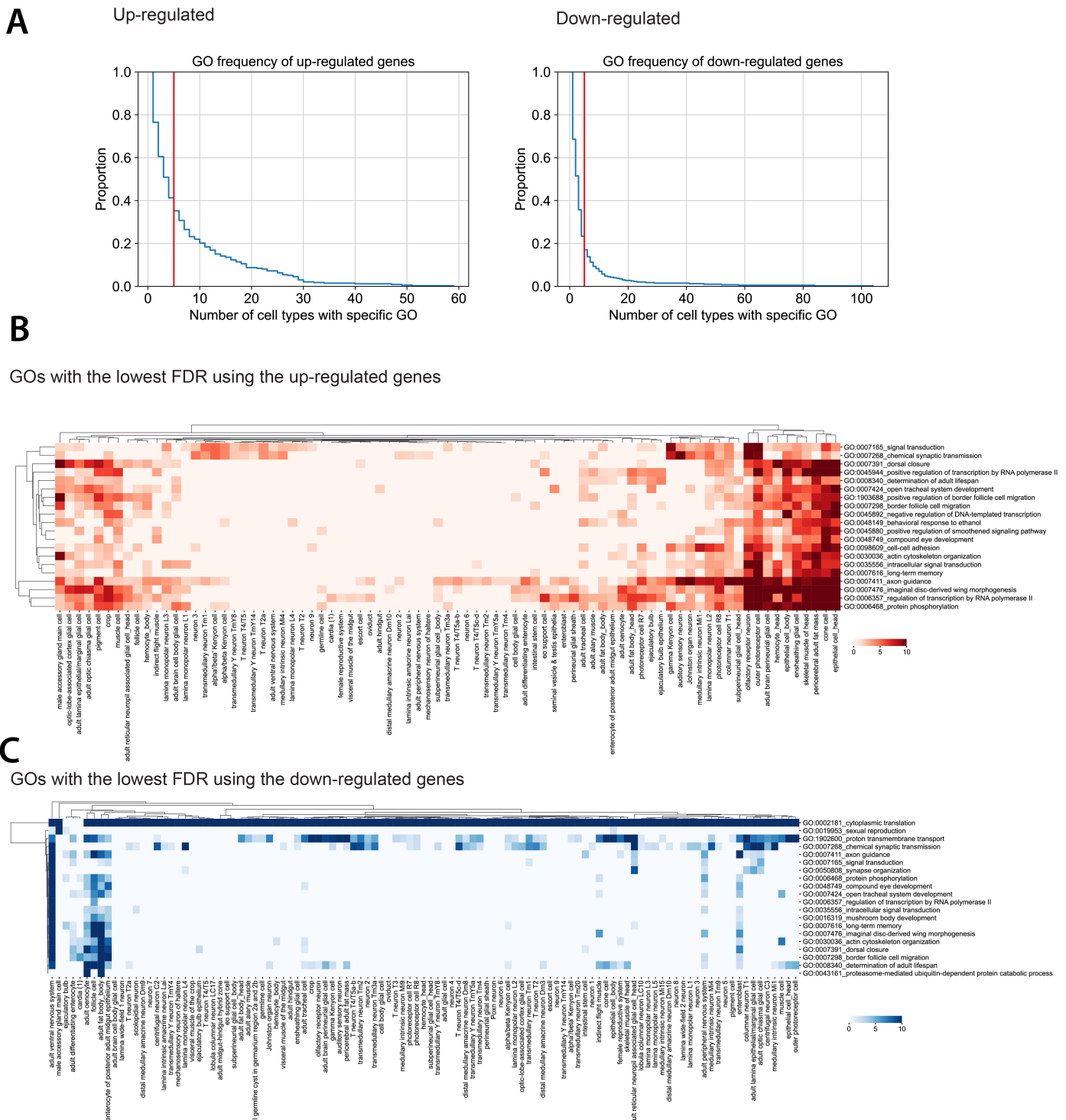


**Fig. S20 GO frequency and the most significant GOs from the up- or down-regulated genes.**

A-B) Up- and down-regulated DEGs are identified by comparing 50d flies to 5d flies. A) GO frequencies from up- or down-regulated genes. GO frequency indicates how many cell types have the corresponding GO. The red line indicates five cell types with the corresponding GO. B) GOs with the lowest FDR from the up-regulated genes. C) GOs with the lowest FDR from the down-regulated genes.

# Figure S21

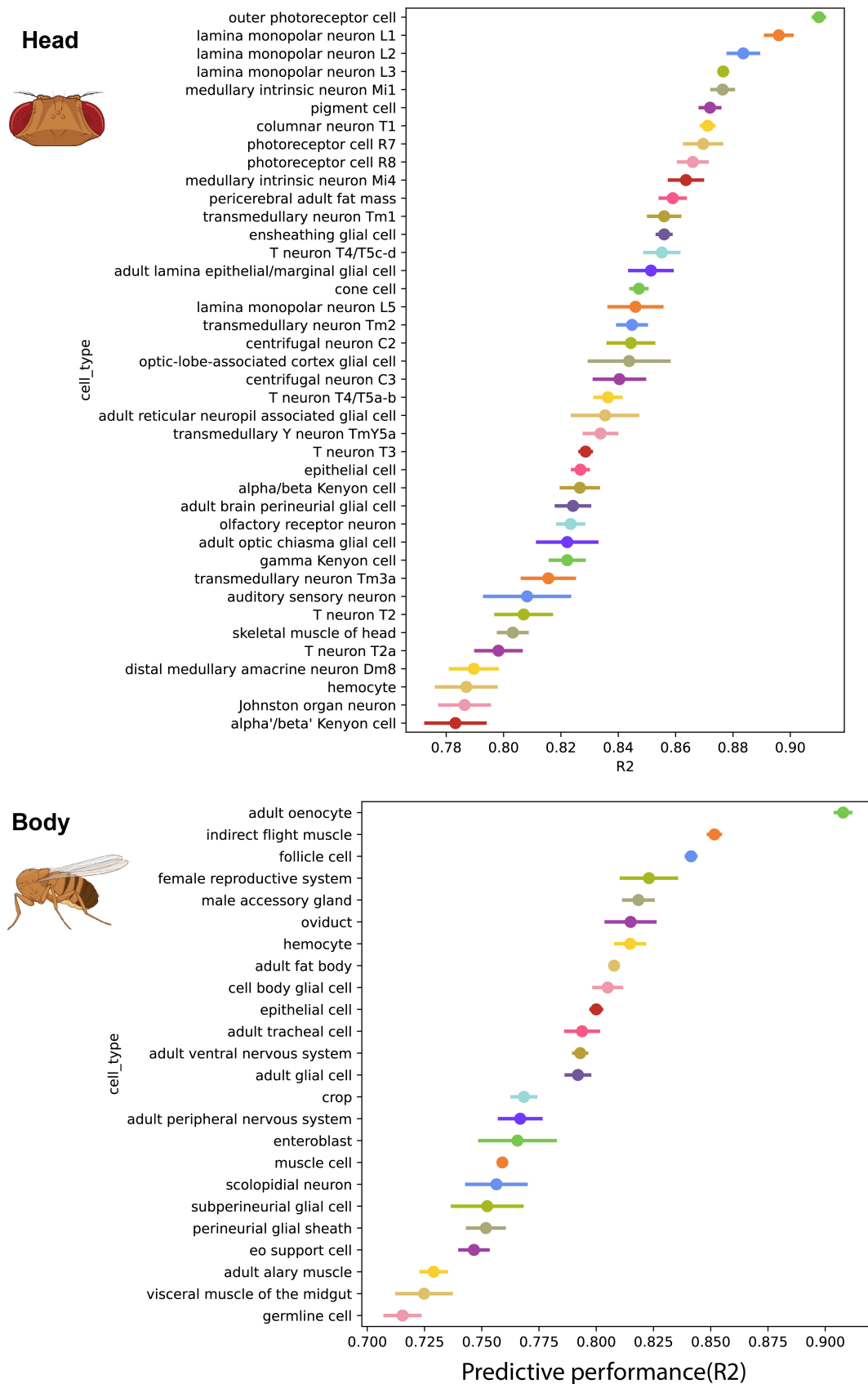
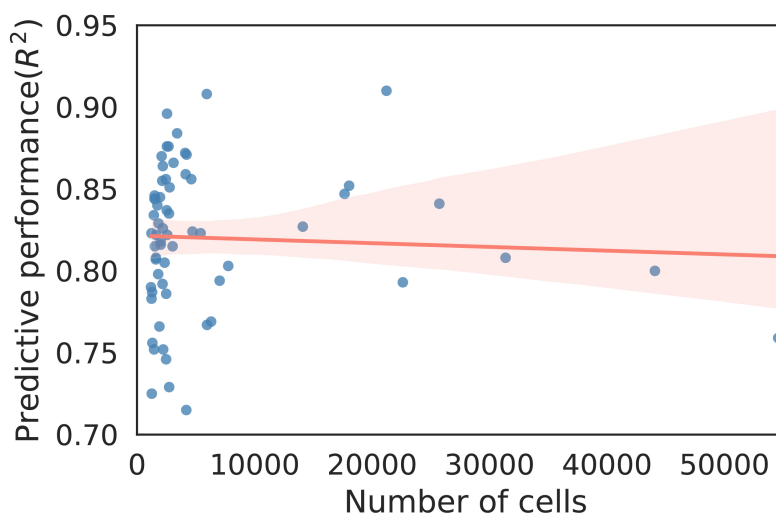


**Fig. S21 Predictive performance of aging clocks.**

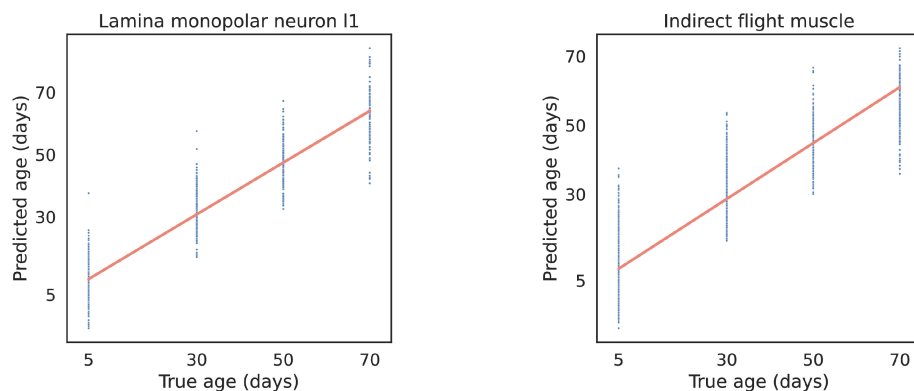
Predictive performances of aging clocks from each cell type. Performances of head and body cell types are shown separately.

# Figure S22

**A**

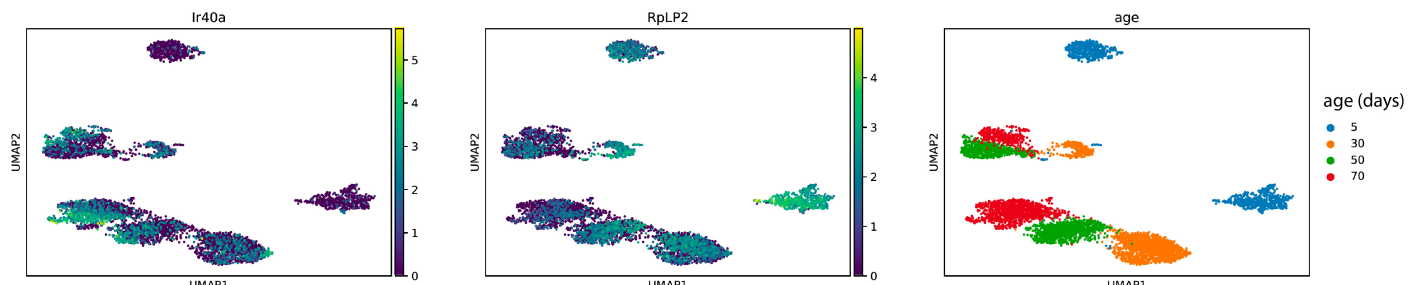


**B**



**C**

### adult\_oenocyte



### Outer photoreceptor cell

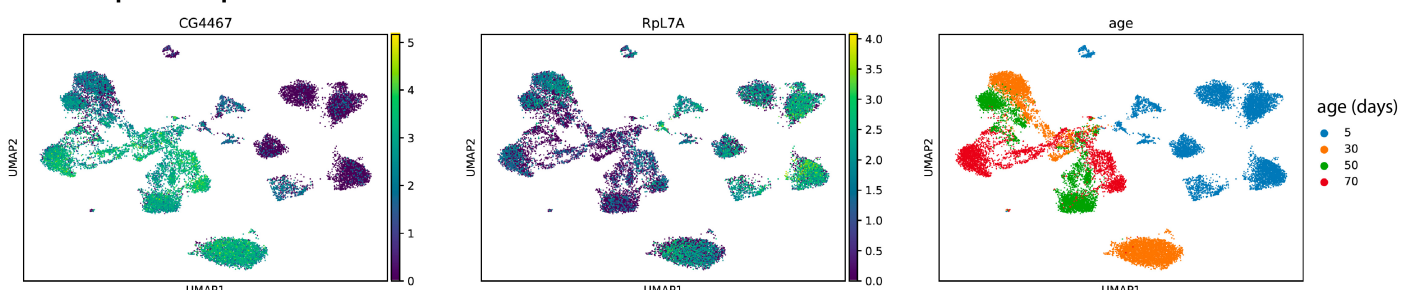


**Fig. S22 Aging clock profiles.**

A) The cell numbers from each cell type are not correlated to the predictive performance. B) Examples of two cell types with good prediction of true age. C) Expression of aging clock genes in two different cell types.

# Figure S23

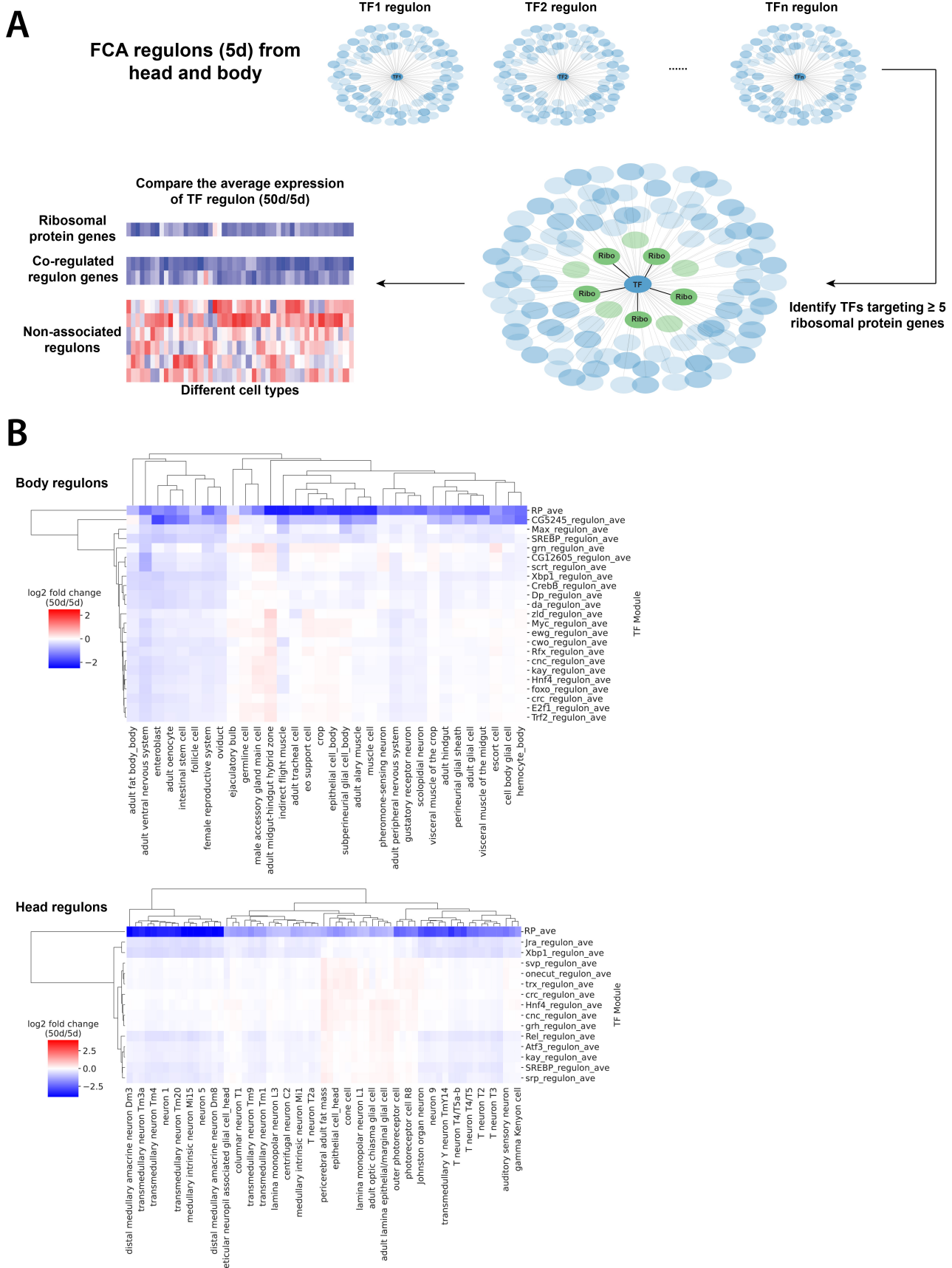


**Fig. S23 Identification of possible TFs regulating the expression of ribosomal protein genes.**

A) The flowchart of identification of possible TFs of ribosomal protein genes. B) The averaged expressions of RP gene-related regulons.

# Figure S24

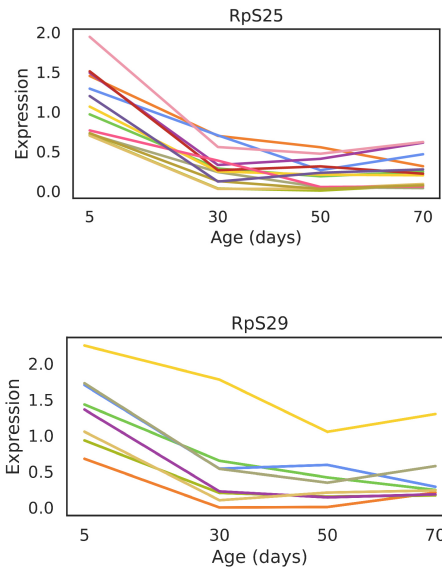
<b>fly_gene</b>	<b>mouse_ortholog</b>	<b># cell types in fly</b>	<b># cell types in mouse</b>
RpL13A	Rpl13a	8	24
RpS25	Rps25	13	18
RpS29	Rps29	5	24
RpS26	Rps26	10	10
RpS21	Rps21	3	15
RpS15	Rps15	15	2
RpS23	Rps23	6	11
RpL27A	Rpl27a	15	1
RpS7	Rps7	13	2
RpL21	Rpl21	11	2
RpL35A	Rpl35a	3	10
RpL14	Rpl14	11	1
RpS12	Rps12	7	5
RpS8	Rps8	11	1
RpL23	Rpl23	8	3
RpL38	Rpl38	1	10
RpL10Ab	Rpl10a	9	1
RpS16	Rps16	6	3
RpS3	Rps3	3	6
sta	Rpsa	7	1
RpL13	Rpl13	3	4
RpL31	Rpl31	4	3
RpS17	Rps17	2	5
RpLP0	Rplp0	4	2
RpS20	Rps20	5	1
RpS24	Rps24	4	1
RpS30	Fau	3	2
ATPsynbeta	Atp5b	2	2
RpL11	Rpl11	3	1
RpS11	Rps11	3	1
RpS6	Rps6	3	1
Hsc70-3	Hspa5	1	2
RpL24	Rpl24	1	1

**Fig. S24 Aging clock genes present in both fly and mouse.**

1-1 orthologs of 33 aging clock genes conserved between fly and mouse. The number of cell types shown in each species indicates that the aging clock genes are detected as aging clock genes in the corresponding number of cell types.

# Figure S25

## Fly ribosomal protein gene



## Mouse ribosomal protein gene

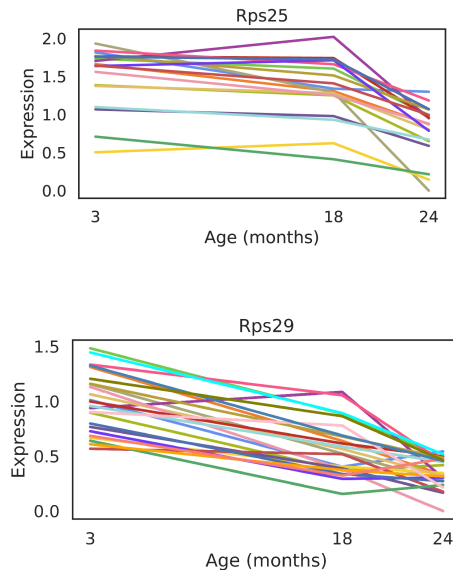
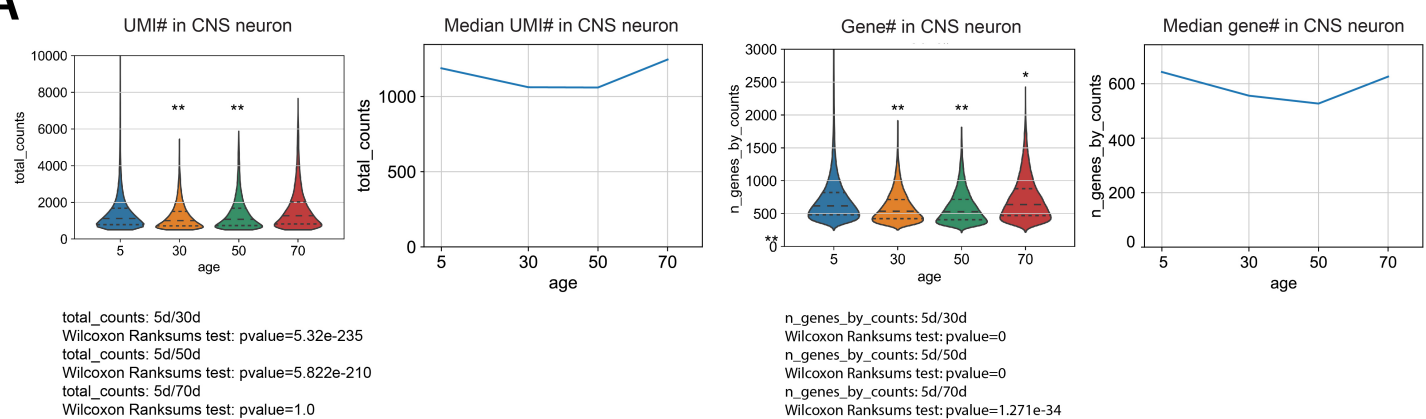


**Fig. S25 Examples of cross-species comparison of aging clock genes.**

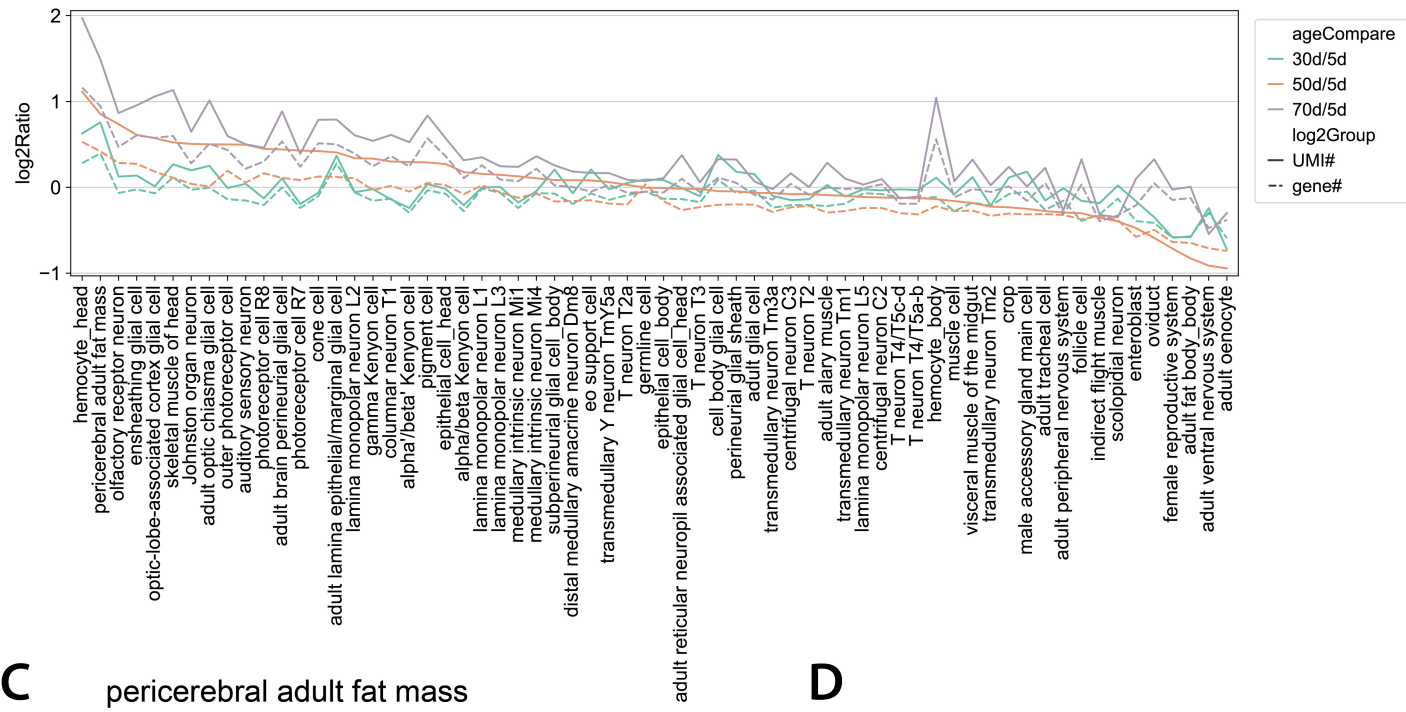
Expression of two orthologous aging clock genes.

# Figure S26

**A**

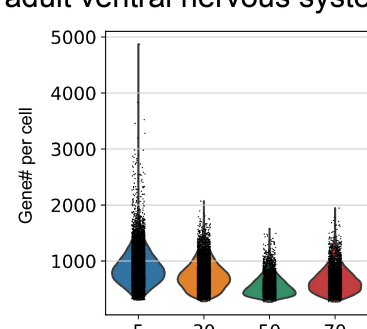
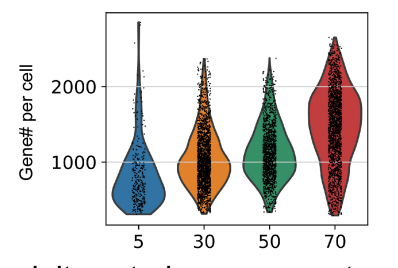


**B**



**C**

pericerebral adult fat mass



**D**

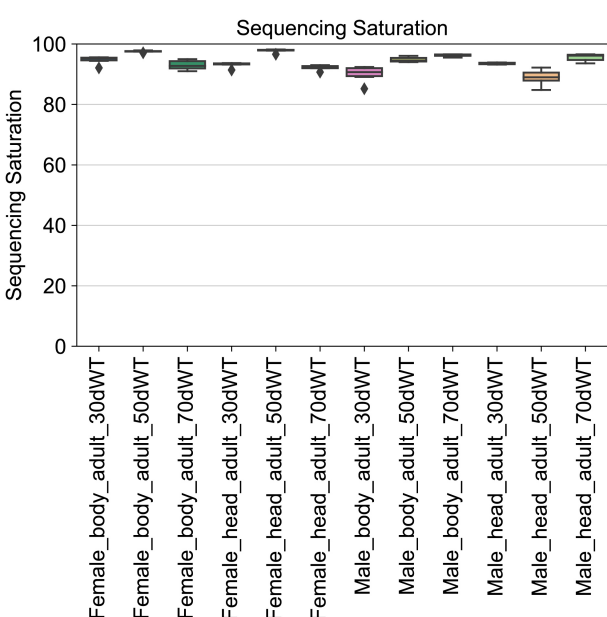


**Fig. S26 Variance of UMI and expressed gene numbers during aging.**

A) Numbers of expressed genes and UMIs per cell are decreased in the aged CNS neurons (30d and 50d). B) Log2 ratio of expressed gene or UMI number per cell during aging. C) Changes of expressed gene number in pericerebral adult fat mass and adult fat body from the body. D) Sequencing saturation of different batches of samples.

# Figure S27

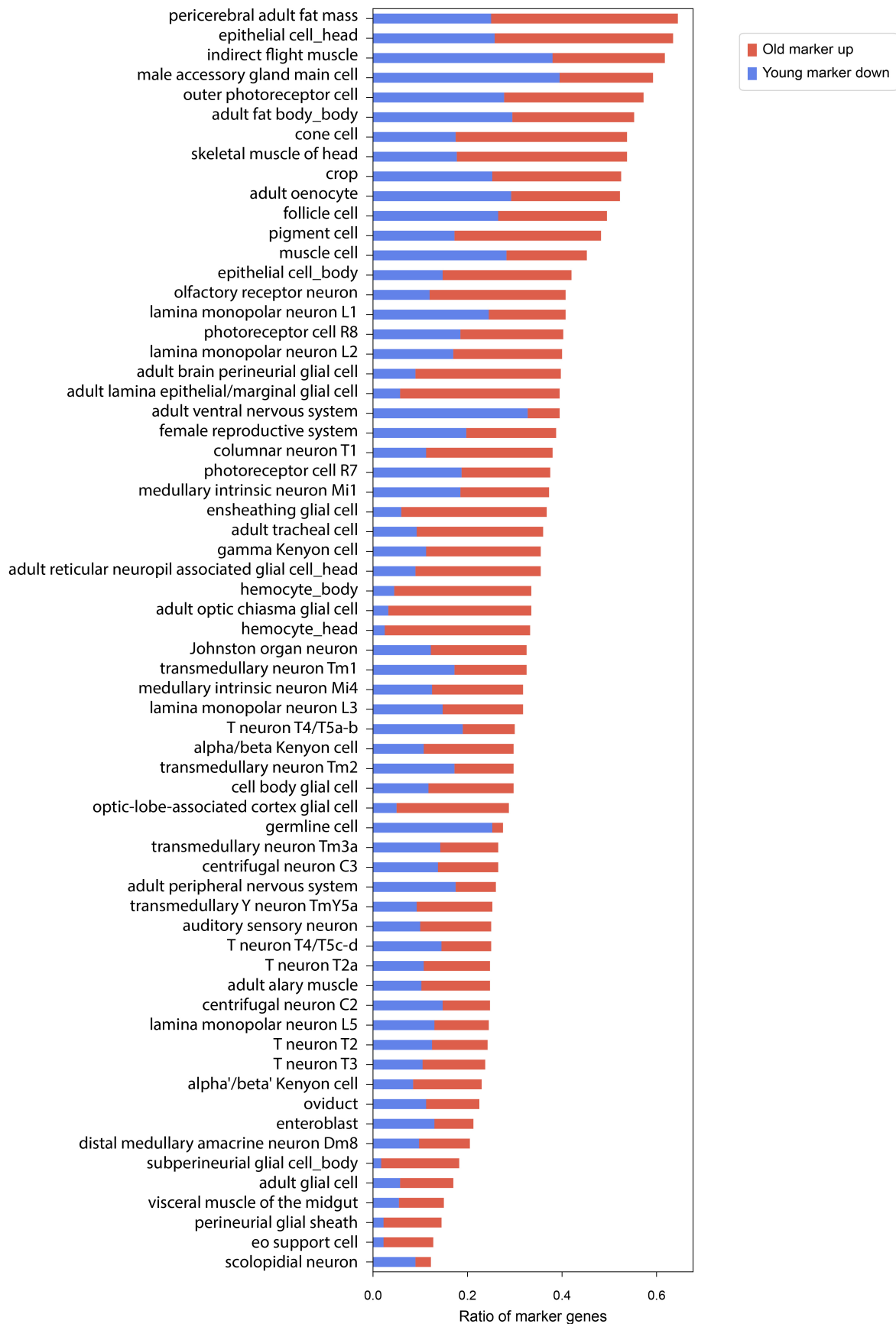


**Fig. S27 Changes of cell-type identity during aging.**

Cell types ranked by the decline of cell-type identity during aging. The decrease of young markers and the increase of old markers are shown separately in each cell type.

# Figure S28

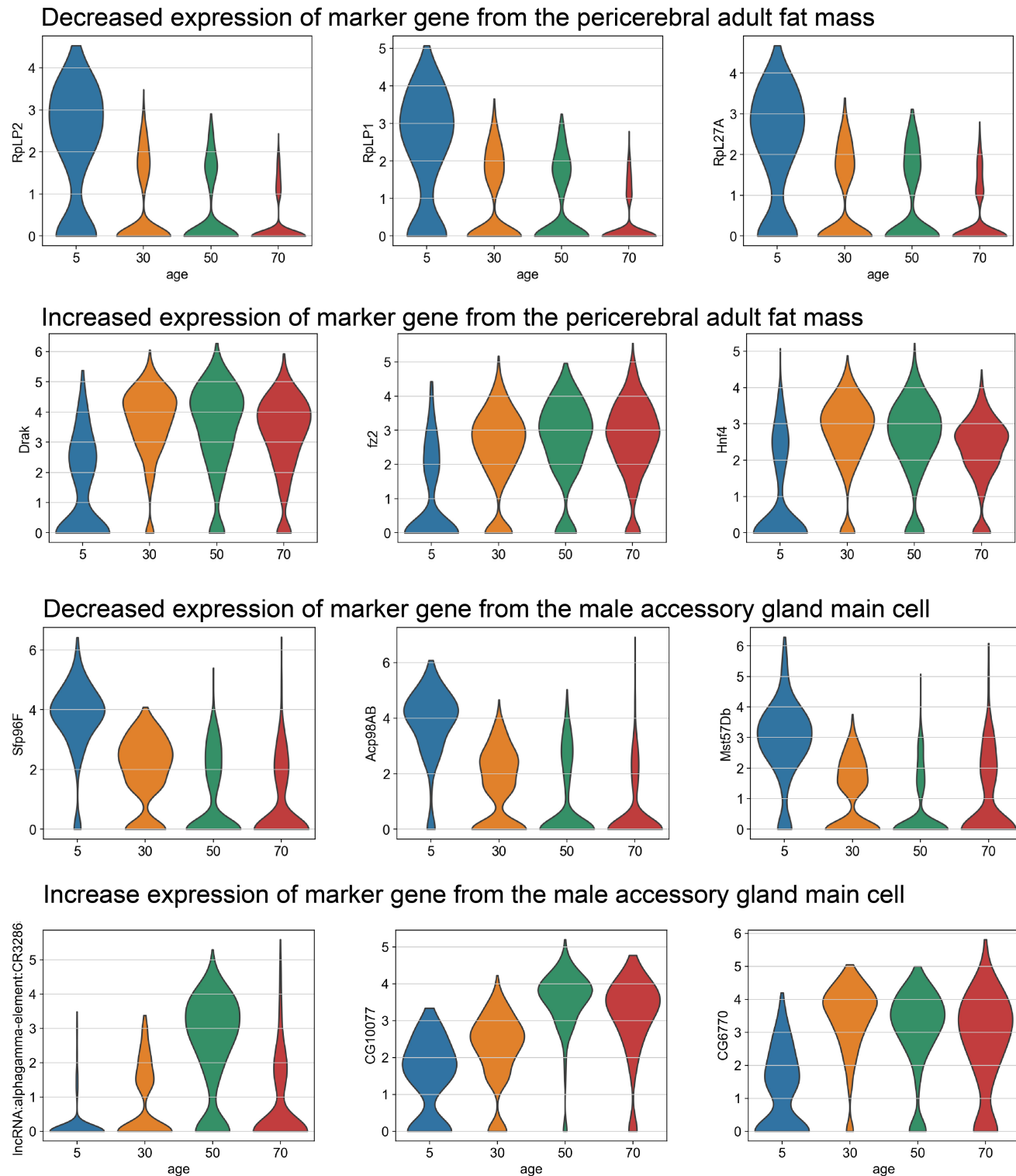


**Fig. S28 Marker genes that affect cell-type identities during aging.**  
Examples of marker genes that caused the decline of cell-type identities.

# Figure S29

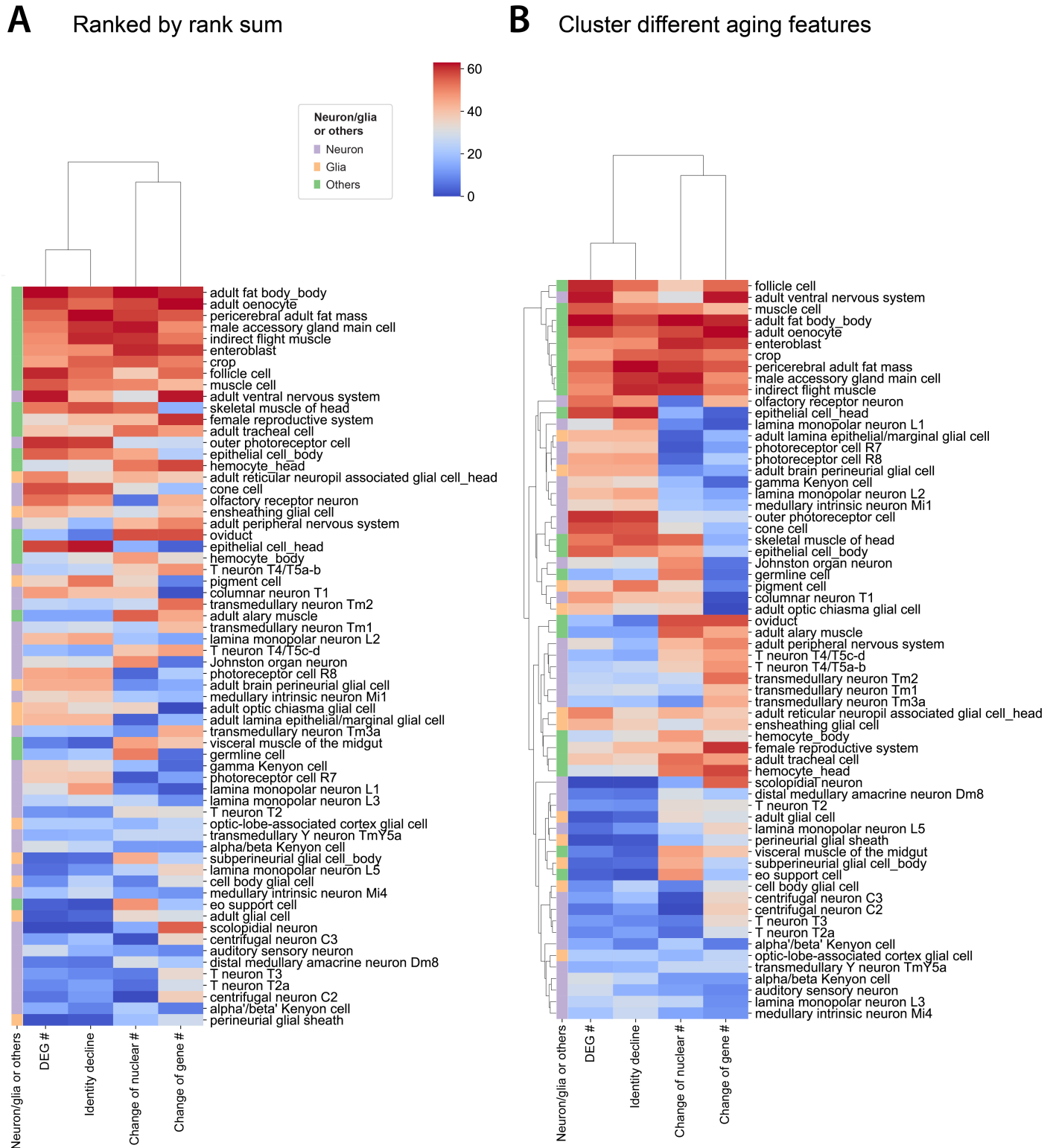


**Fig. S29 Rank sums of different aging features.**

A) Cell types ranked by the sum of different aging feature scores. B) Clustering of rank sum scores across different cell types.

# Figure S30

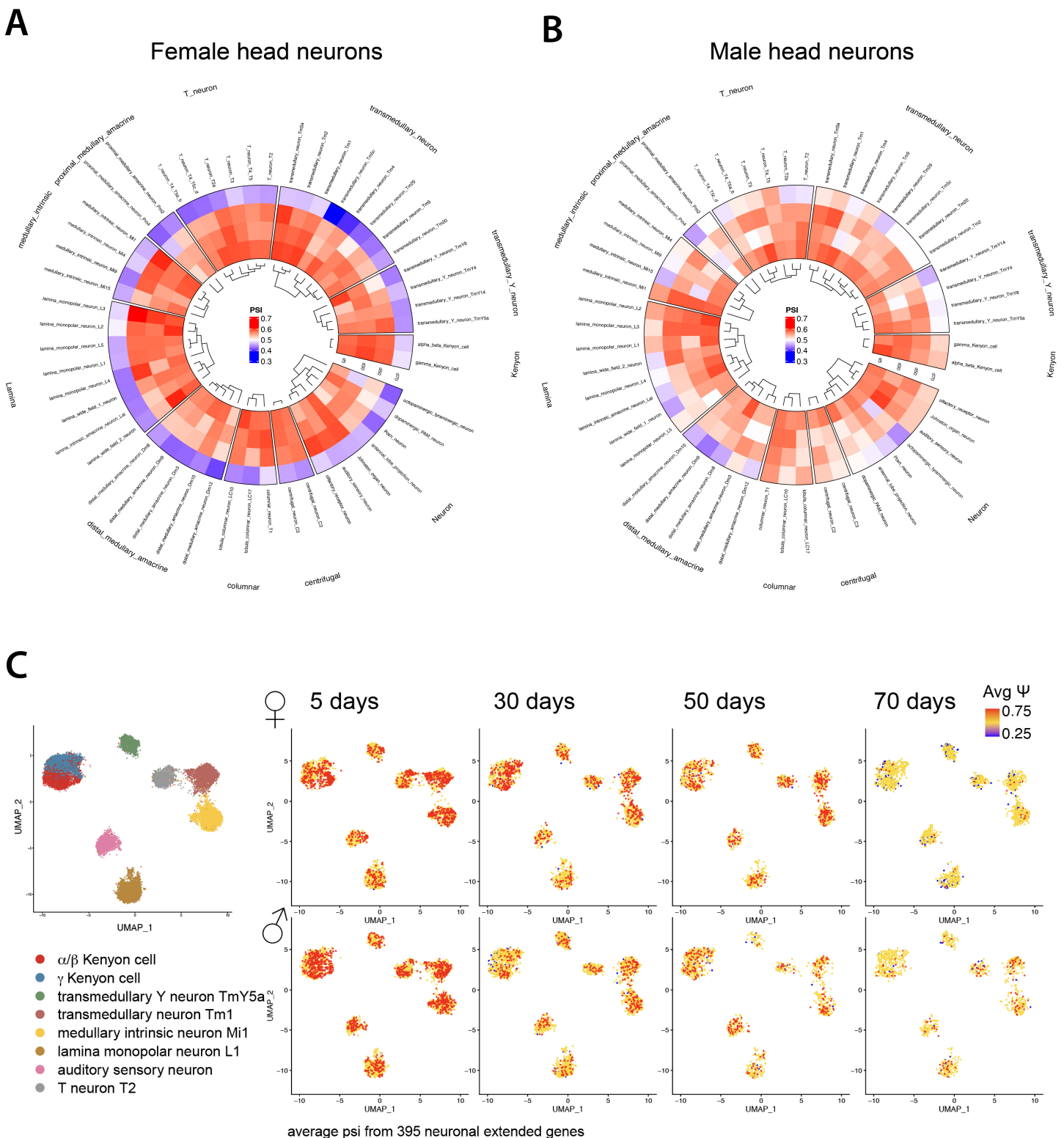


**Fig. S30 Comparison of alternative polyadenylation (APA) scores across different ages.**

A-B) The circular heatmaps summarize APA trends from the annotated neuronal extended genes across different time points in females (A) and males (B). We use the LABRATsc package to calculate  $\psi$  and the average value for 391 neuronal extended genes, which are plotted in each of the neuronal types from the AFCA head data. C) UMAP of different neuronal types designated by the AFCA. Average 3' isoform usage of 391 neural extended genes is plotted in individual cells by different aging time points. Both analyses show that neuronal extended 3' isoforms are progressively depleted during aging. This phenotype is stronger in females at 70d.

**Movies S1-S3.** Three examples of three-dimensional (3D) reconstructions of two attached nuclei in the same fat body cell. The attached nuclei are stained by DAPI and LamC. The membranes of fat body cells are labeled by *cg-GAL4 > UAS-CD8GFP*.

## References and Notes

1. C. López-Otín, M. A. Blasco, L. Partridge, M. Serrano, G. Kroemer, The hallmarks of aging. *Cell* **153**, 1194–1217 (2013). [doi:10.1016/j.cell.2013.05.039](https://doi.org/10.1016/j.cell.2013.05.039) [Medline](#)
2. T. Niccoli, L. Partridge, Ageing as a risk factor for disease. *Curr. Biol.* **22**, R741–R752 (2012). [doi:10.1016/j.cub.2012.07.024](https://doi.org/10.1016/j.cub.2012.07.024) [Medline](#)
3. D. Harman, The free radical theory of aging. *Antioxid. Redox Signal.* **5**, 557–561 (2003). [doi:10.1089/152308603770310202](https://doi.org/10.1089/152308603770310202) [Medline](#)
4. H. J. Bellen, C. Tong, H. Tsuda, 100 years of *Drosophila* research and its impact on vertebrate neuroscience: A history lesson for the future. *Nat. Rev. Neurosci.* **11**, 514–522 (2010). [doi:10.1038/nrn2839](https://doi.org/10.1038/nrn2839) [Medline](#)
5. D. Baldridge, M. F. Wangler, A. N. Bowman, S. Yamamoto, T. Schedl, S. C. Pak, J. H. Postlethwait, J. Shin, L. Solnica-Krezel, H. J. Bellen, M. Westerfield; Undiagnosed Diseases Network, Model organisms contribute to diagnosis and discovery in the undiagnosed diseases network: Current state and a future vision. *Orphanet J. Rare Dis.* **16**, 206 (2021). [doi:10.1186/s13023-021-01839-9](https://doi.org/10.1186/s13023-021-01839-9) [Medline](#)
6. M. S. Grotewiel, I. Martin, P. Bhandari, E. Cook-Wiens, Functional senescence in *Drosophila melanogaster*. *Ageing Res. Rev.* **4**, 372–397 (2005). [doi:10.1016/j.arr.2005.04.001](https://doi.org/10.1016/j.arr.2005.04.001) [Medline](#)
7. H. Li, J. Janssens, M. De Waegeneer, S. S. Kolluru, K. Davie, V. Gardeux, W. Saelens, F. P. A. David, M. Brbić, K. Spanier, J. Leskovec, C. N. McLaughlin, Q. Xie, R. C. Jones, K. Brueckner, J. Shim, S. G. Tattikota, F. Schnorrer, K. Rust, T. G. Nystul, Z. Carvalho-Santos, C. Ribeiro, S. Pal, S. Mahadevaraju, T. M. Przytycka, A. M. Allen, S. F. Goodwin, C. W. Berry, M. T. Fuller, H. White-Cooper, E. L. Matunis, S. DiNardo, A. Galenza, L. E. O'Brien, J. A. T. Dow, H. Jasper, B. Oliver, N. Perrimon, B. Deplancke, S. R. Quake, L. Luo, S. Aerts, D. Agarwal, Y. Ahmed-Braimah, M. Arbeitman, M. M. Ariss, J. Augsburger, K. Ayush, C. C. Baker, T. Banisch, K. Birker, R. Bodmer, B. Bolival, S. E. Brantley, J. A. Brill, N. C. Brown, N. A. Buehner, X. T. Cai, R. Cardoso-Figueiredo, F. Casares, A. Chang, T. R. Clandinin, S. Crasta, C. Desplan, A. M. Detweiler, D. B. Dhakan, E. Donà, S. Engert, S. Floc'hlay, N. George, A. J. González-Segarra, A. K. Groves, S. Gumbin, Y. Guo, D. E. Harris, Y. Heifetz, S. L. Holtz, F. Horns, B. Hudry, R.-J. Hung, Y. N. Jan, J. S. Jaszcak, G. S. X. E. Jefferis, J. Karkanias, T. L. Karr, N. S. Katheder, J. Kezos, A. A. Kim, S. K. Kim, L. Kockel, N. Konstantinides, T. B. Kornberg, H. M. Krause, A. T. Labott, M. Latsbury, R. Lehmann, S. Leinwand, J. Li, J. S. S. Li, K. Li, L. Li, T. Li, M. Litovchenko, H.-H. Liu, Y. Liu, T.-C. Lu, J. Manning, A. Mase, M. Matera-Vatnick, N. R. Matias, C. E. McDonough-Goldstein, A. McGeever, A. D. McLachlan, P. Moreno-Roman, N. Neff, M. Neville, S. Ngo, T. Nielsen, C. E. O'Brien, D. Osumi-Sutherland, M. N. Özel, I. Papatheodorou, M. Petkovic, C. Pilgrim, A. O. Pisco, C. Reisenman, E. N. Sanders, G. Dos Santos, K. Scott, A. Sherlekhar, P. Shiu, D. Sims, R. V. Sit, M. Slaidina, H. E. Smith, G. Sterne, Y.-H. Su, D. Sutton, M. Tamayo, M. Tan, I. Tastekin, C. Treiber, D. Vacek, G. Vogler, S. Waddell, W. Wang, R. I. Wilson, M. F. Wolfner, Y. E. Wong, A. Xie, J. Xu, S. Yamamoto, J. Yan, Z. Yao, K. Yoda, R. Zhu, R. P. Zinzen; FCA Consortium, Fly Cell

Atlas: A single-nucleus transcriptomic atlas of the adult fruit fly. *Science* **375**, eabk2432 (2022). [doi:10.1126/science.abk2432](https://doi.org/10.1126/science.abk2432) [Medline](#)

8. K. Davie, J. Janssens, D. Koldere, M. De Waegeneer, U. Pech, Ł. Kreft, S. Aibar, S. Makhzami, V. Christiaens, C. Bravo González-Blas, S. Poovathingal, G. Hulselmans, K. I. Spanier, T. Moerman, B. Vanspauwen, S. Geurs, T. Voet, J. Lammertyn, B. Thienpont, S. Liu, N. Konstantinides, M. Fiers, P. Verstreken, S. Aerts, A single-cell transcriptome atlas of the aging *Drosophila* brain. *Cell* **174**, 982–998.e20 (2018). [doi:10.1016/j.cell.2018.05.057](https://doi.org/10.1016/j.cell.2018.05.057) [Medline](#)
9. J. Janssens, S. Aibar, I. I. Taskiran, J. N. Ismail, A. E. Gomez, G. Aughey, K. I. Spanier, F. V. De Rop, C. B. González-Blas, M. Dionne, K. Grimes, X. J. Quan, D. Papasokrati, G. Hulselmans, S. Makhzami, M. De Waegeneer, V. Christiaens, T. Southall, S. Aerts, Decoding gene regulation in the fly brain. *Nature* **601**, 630–636 (2022). [doi:10.1038/s41586-021-04262-z](https://doi.org/10.1038/s41586-021-04262-z) [Medline](#)
10. H. Zeng, What is a cell type and how to define it? *Cell* **185**, 2739–2755 (2022). [doi:10.1016/j.cell.2022.06.031](https://doi.org/10.1016/j.cell.2022.06.031) [Medline](#)
11. G. La Manno, K. Siletti, A. Furlan, D. Gyllborg, E. Vinsland, A. Mossi Albiach, C. Mattsson Langseth, I. Khven, A. R. Lederer, L. M. Dratva, A. Johnsson, M. Nilsson, P. Lönnérberg, S. Linnarsson, Molecular architecture of the developing mouse brain. *Nature* **596**, 92–96 (2021). [doi:10.1038/s41586-021-03775-x](https://doi.org/10.1038/s41586-021-03775-x) [Medline](#)
12. H. Li, H. Jasper, Gastrointestinal stem cells in health and disease: From flies to humans. *Dis. Model. Mech.* **9**, 487–499 (2016). [doi:10.1242/dmm.024232](https://doi.org/10.1242/dmm.024232) [Medline](#)
13. H. Jasper, Intestinal stem cell aging: origins and interventions. *Annu. Rev. Physiol.* **82**, 203–226 (2020). [doi:10.1146/annurev-physiol-021119-034359](https://doi.org/10.1146/annurev-physiol-021119-034359) [Medline](#)
14. C. A. Micchelli, N. Perrimon, Evidence that stem cells reside in the adult *Drosophila* midgut epithelium. *Nature* **439**, 475–479 (2006). [doi:10.1038/nature04371](https://doi.org/10.1038/nature04371) [Medline](#)
15. B. Ohlstein, A. Spradling, The adult *Drosophila* posterior midgut is maintained by pluripotent stem cells. *Nature* **439**, 470–474 (2006). [doi:10.1038/nature04333](https://doi.org/10.1038/nature04333) [Medline](#)
16. F. A. Wolf, F. K. Hamey, M. Plass, J. Solana, J. S. Dahlin, B. Göttgens, N. Rajewsky, L. Simon, F. J. Theis, PAGA: Graph abstraction reconciles clustering with trajectory inference through a topology preserving map of single cells. *Genome Biol.* **20**, 59 (2019). [doi:10.1186/s13059-019-1663-x](https://doi.org/10.1186/s13059-019-1663-x) [Medline](#)
17. M. Jacomy, T. Venturini, S. Heymann, M. Bastian, ForceAtlas2, a continuous graph layout algorithm for handy network visualization designed for the Gephi software. *PLOS ONE* **9**, e98679 (2014). [doi:10.1371/journal.pone.0098679](https://doi.org/10.1371/journal.pone.0098679) [Medline](#)
18. I. A. Rodriguez-Fernandez, H. M. Tauc, H. Jasper, Hallmarks of aging *Drosophila* intestinal stem cells. *Mech. Ageing Dev.* **190**, 111285 (2020). [doi:10.1016/j.mad.2020.111285](https://doi.org/10.1016/j.mad.2020.111285) [Medline](#)
19. A. Rezaei, M. S. Krishna, H. T. Santhosh, Male age affects female mate preference, quantity of accessory gland proteins, and sperm traits and female fitness in *D. melanogaster*. *Zoolog. Sci.* **32**, 16–24 (2015). [doi:10.2108/zs140121](https://doi.org/10.2108/zs140121) [Medline](#)

20. B. Biteau, C. E. Hochmuth, H. Jasper, JNK activity in somatic stem cells causes loss of tissue homeostasis in the aging *Drosophila* gut. *Cell Stem Cell* **3**, 442–455 (2008). [doi:10.1016/j.stem.2008.07.024](https://doi.org/10.1016/j.stem.2008.07.024) [Medline](#)
21. J. C. Regan, M. Khericha, A. J. Dobson, E. Bolukbasi, N. Rattanavirotkul, L. Partridge, Sex difference in pathology of the ageing gut mediates the greater response of female lifespan to dietary restriction. *eLife* **5**, e10956 (2016). [doi:10.7554/eLife.10956](https://doi.org/10.7554/eLife.10956) [Medline](#)
22. E. L. Arrese, J. L. Soulages, Insect fat body: Energy, metabolism, and regulation. *Annu. Rev. Entomol.* **55**, 207–225 (2010). [doi:10.1146/annurev-ento-112408-085356](https://doi.org/10.1146/annurev-ento-112408-085356) [Medline](#)
23. V. P. Losick, D. T. Fox, A. C. Spradling, Polyploidization and cell fusion contribute to wound healing in the adult *Drosophila* epithelium. *Curr. Biol.* **23**, 2224–2232 (2013). [doi:10.1016/j.cub.2013.09.029](https://doi.org/10.1016/j.cub.2013.09.029) [Medline](#)
24. E. M. Lucchetta, B. Ohlstein, Amitosis of polyploid cells regenerates functional stem cells in the *Drosophila* intestine. *Cell Stem Cell* **20**, 609–620.e6 (2017). [doi:10.1016/j.stem.2017.02.012](https://doi.org/10.1016/j.stem.2017.02.012) [Medline](#)
25. T. J. Doherty, Invited review: Aging and sarcopenia. *J. Appl. Physiol.* **95**, 1717–1727 (2003). [doi:10.1152/japplphysiol.00347.2003](https://doi.org/10.1152/japplphysiol.00347.2003) [Medline](#)
26. H.-J. Jeon, Y.-S. Kim, J.-S. Park, J.-H. Pyo, H.-J. Na, I.-J. Kim, C.-M. Kim, H. Y. Chung, N. D. Kim, R. Arking, M.-A. Yoo, Age-related change in γH2AX of *Drosophila* muscle: Its significance as a marker for muscle damage and longevity. *Biogerontology* **16**, 503–516 (2015). [doi:10.1007/s10522-015-9573-0](https://doi.org/10.1007/s10522-015-9573-0) [Medline](#)
27. Tabula Muris Consortium, A single-cell transcriptomic atlas characterizes ageing tissues in the mouse. *Nature* **583**, 590–595 (2020). [doi:10.1038/s41586-020-2496-1](https://doi.org/10.1038/s41586-020-2496-1) [Medline](#)
28. H. Hall, P. Medina, D. A. Cooper, S. E. Escobedo, J. Rounds, K. J. Brennan, C. Vincent, P. Miura, R. Doerge, V. M. Weake, Transcriptome profiling of aging *Drosophila* photoreceptors reveals gene expression trends that correlate with visual senescence. *BMC Genomics* **18**, 894 (2017). [doi:10.1186/s12864-017-4304-3](https://doi.org/10.1186/s12864-017-4304-3) [Medline](#)
29. Y. Gonskikh, N. Polacek, Alterations of the translation apparatus during aging and stress response. *Mech. Ageing Dev.* **168**, 30–36 (2017). [doi:10.1016/j.mad.2017.04.003](https://doi.org/10.1016/j.mad.2017.04.003) [Medline](#)
30. H. Ruhmann, M. Koppik, M. F. Wolfner, C. Fricke, The impact of ageing on male reproductive success in *Drosophila melanogaster*. *Exp. Gerontol.* **103**, 1–10 (2018). [doi:10.1016/j.exger.2017.12.013](https://doi.org/10.1016/j.exger.2017.12.013) [Medline](#)
31. S. Horvath, K. Raj, DNA methylation-based biomarkers and the epigenetic clock theory of ageing. *Nat. Rev. Genet.* **19**, 371–384 (2018). [doi:10.1038/s41576-018-0004-3](https://doi.org/10.1038/s41576-018-0004-3) [Medline](#)
32. M. T. Buckley, E. D. Sun, B. M. George, L. Liu, N. Schaum, L. Xu, J. M. Reyes, M. A. Goodell, I. L. Weissman, T. Wyss-Coray, T. A. Rando, A. Brunet, Cell-type-specific aging clocks to quantify aging and rejuvenation in neurogenic regions of the brain. *Nat. Aging* **3**, 121–137 (2023). [doi:10.1038/s43587-022-00335-4](https://doi.org/10.1038/s43587-022-00335-4) [Medline](#)
33. H. Zou, T. Hastie, Regularization and variable selection via the elastic net. *J. R. Stat. Soc. Series B Stat. Methodol.* **67**, 301–320 (2005). [doi:10.1111/j.1467-9868.2005.00503.x](https://doi.org/10.1111/j.1467-9868.2005.00503.x)

34. A. C. Ghosh, S. G. Tattikota, Y. Liu, A. Comjean, Y. Hu, V. Barrera, S. J. Ho Sui, N. Perrimon, *Drosophila* PDGF/VEGF signaling from muscles to hepatocyte-like cells protects against obesity. *eLife* **9**, e56969 (2020). [doi:10.7554/eLife.56969](https://doi.org/10.7554/eLife.56969) Medline
35. N. Basisty, J. G. Meyer, B. Schilling, Protein turnover in aging and longevity. *Proteomics* **18**, e1700108 (2018). [doi:10.1002/pmic.201700108](https://doi.org/10.1002/pmic.201700108) Medline
36. S. Aibar, C. B. González-Blas, T. Moerman, V. A. Huynh-Thu, H. Imrichova, G. Hulselmans, F. Rambow, J.-C. Marine, P. Geurts, J. Aerts, J. van den Oord, Z. K. Atak, J. Wouters, S. Aerts, SCENIC: Single-cell regulatory network inference and clustering. *Nat. Methods* **14**, 1083–1086 (2017). [doi:10.1038/nmeth.4463](https://doi.org/10.1038/nmeth.4463) Medline
37. H. Izgi, D. Han, U. Isildak, S. Huang, E. Kocabiyik, P. Khaitovich, M. Somel, H. M. Dönertaş, Inter-tissue convergence of gene expression during ageing suggests age-related loss of tissue and cellular identity. *eLife* **11**, e68048 (2022). [doi:10.7554/eLife.68048](https://doi.org/10.7554/eLife.68048) Medline
38. S. M. Gao, Y. Qi, Q. Zhang, A. S. Mohammed, Y.-T. Lee, Y. Guan, H. Li, Y. Fu, M. C. Wang, Aging atlas reveals cell-type-specific regulation of pro-longevity strategies. bioRxiv 2023.02.28.530490 [Preprint] (2023). <https://doi.org/10.1101/2023.02.28.530490>.
39. A. E. Roux, H. Yuan, K. Podshivalova, D. Hendrickson, R. Kerr, C. Kenyon, D. R. Kelley, The complete cell atlas of an aging multicellular organism. bioRxiv 2022.06.15.496201 [Preprint] (2022). <https://doi.org/10.1101/2022.06.15.496201>.
40. A. Sziraki, Z. Lu, J. Lee, G. Banyai, S. Anderson, A. Abdulraouf, E. Metzner, A. Liao, A. Epstein, Z. Xu, Z. Zhang, L. Gan, P. T. Nelson, W. Zhou, J. Cao, A global view of aging and Alzheimer's pathogenesis-associated cell population dynamics and molecular signatures in the human and mouse brains. bioRxiv 2022.09.28.509825 [Preprint] (2022). <https://doi.org/10.1101/2022.09.28.509825>.
41. R. Wang, P. Zhang, J. Wang, L. Ma, W. e, S. Suo, M. Jiang, J. Li, H. Chen, H. Sun, L. Fei, Z. Zhou, Y. Zhou, Y. Chen, W. Zhang, X. Wang, Y. Mei, Z. Sun, C. Yu, J. Shao, Y. Fu, Y. Xiao, F. Ye, X. Fang, H. Wu, Q. Guo, X. Fang, X. Li, X. Gao, D. Wang, P.-F. Xu, R. Zeng, G. Xu, L. Zhu, L. Wang, J. Qu, D. Zhang, H. Ouyang, H. Huang, M. Chen, S.-C. Ng, G.-H. Liu, G.-C. Yuan, G. Guo, X. Han, Construction of a cross-species cell landscape at single-cell level. *Nucleic Acids Res.* **51**, 501–516 (2023). [doi:10.1093/nar/gkac633](https://doi.org/10.1093/nar/gkac633) Medline
42. H. Chen, X. Zheng, Y. Zheng, Age-associated loss of lamin-B leads to systemic inflammation and gut hyperplasia. *Cell* **159**, 829–843 (2014). [doi:10.1016/j.cell.2014.10.028](https://doi.org/10.1016/j.cell.2014.10.028) Medline
43. M. J. Bertram, G. A. Akerkar, R. L. Ard, C. Gonzalez, M. F. Wolfner, Cell type-specific gene expression in the *Drosophila melanogaster* male accessory gland. *Mech. Dev.* **38**, 33–40 (1992). [doi:10.1016/0925-4773\(92\)90036-J](https://doi.org/10.1016/0925-4773(92)90036-J) Medline
44. A. M. Box, S. J. Church, S. Nandakumar, D. Prasad, A. Afrakhteh, R. S. Taichman, L. Buttitta, Endocycles support tissue growth and regeneration of the adult *Drosophila* accessory gland. bioRxiv 719013 [Preprint] (2022). <https://doi.org/10.1101/719013>.

45. Y. Unhavaithaya, T. L. Orr-Weaver, Polyploidization of glia in neural development links tissue growth to blood-brain barrier integrity. *Genes Dev.* **26**, 31–36 (2012). [doi:10.1101/gad.177436.111](https://doi.org/10.1101/gad.177436.111) [Medline](#)
46. T. Gehrmann, J. F. Pelkmans, R. A. Ohm, A. M. Vos, A. S. M. Sonnenberg, J. J. P. Baars, H. A. B. Wösten, M. J. T. Reinders, T. Abeel, Nucleus-specific expression in the multinuclear mushroom-forming fungus *Agaricus bisporus* reveals different nuclear regulatory programs. *Proc. Natl. Acad. Sci. U.S.A.* **115**, 4429–4434 (2018). [doi:10.1073/pnas.1721381115](https://doi.org/10.1073/pnas.1721381115) [Medline](#)
47. P. von Aderkas, G. Rouault, R. Wagner, S. Chiwocha, A. Roques, Multinucleate storage cells in Douglas-fir (*Pseudotsuga menziesii* (Mirbel) Franco) and the effect of seed parasitism by the chalcid *Megastigmus spermotrophus* Wachtl. *Heredity* **94**, 616–622 (2005). [doi:10.1038/sj.hdy.6800670](https://doi.org/10.1038/sj.hdy.6800670) [Medline](#)
48. H.-Z. Chen, M. M. Ouseph, J. Li, T. Pécot, V. Chokshi, L. Kent, S. Bae, M. Byrne, C. Duran, G. Comstock, P. Trikha, M. Mair, S. Senapati, C. K. Martin, S. Gandhi, N. Wilson, B. Liu, Y.-W. Huang, J. C. Thompson, S. Raman, S. Singh, M. Leone, R. Machiraju, K. Huang, X. Mo, S. Fernandez, I. Kalaszczynska, D. J. Wolgemuth, P. Sicinski, T. Huang, V. Jin, G. Leone, Canonical and atypical E2Fs regulate the mammalian endocycle. *Nat. Cell Biol.* **14**, 1192–1202 (2012). [doi:10.1038/ncb2595](https://doi.org/10.1038/ncb2595) [Medline](#)
49. B. N. Kudryavtsev, M. V. Kudryavtseva, G. A. Sakuta, G. I. Stein, Human hepatocyte polyploidization kinetics in the course of life cycle. *Virchows Arch. B Cell Pathol. Incl. Mol. Pathol.* **64**, 387–393 (1993). [doi:10.1007/BF02915139](https://doi.org/10.1007/BF02915139) [Medline](#)
50. S. Lee, Y.-C. Chen, A. E. Gillen, J. M. Taliaferro, B. Deplancke, H. Li, E. C. Lai; FCA Consortium, Diverse cell-specific patterns of alternative polyadenylation in *Drosophila*. *Nat. Commun.* **13**, 5372 (2022). [doi:10.1038/s41467-022-32305-0](https://doi.org/10.1038/s41467-022-32305-0) [Medline](#)
51. X. Zhao, J. Karpac, Glutamate metabolism directs energetic trade-offs to shape host-pathogen susceptibility in *Drosophila*. *Cell Metab.* **33**, 2428–2444.e8 (2021). [doi:10.1016/j.cmet.2021.10.003](https://doi.org/10.1016/j.cmet.2021.10.003) [Medline](#)
52. N. Chatterjee, N. Perrimon, What fuels the fly: Energy metabolism in *Drosophila* and its application to the study of obesity and diabetes. *Sci. Adv.* **7**, eabg4336 (2021). [doi:10.1126/sciadv.abg4336](https://doi.org/10.1126/sciadv.abg4336) [Medline](#)
53. T.-C. Lu, MeshifLu/AFCA: AFCA\_v1.0 (AFCA\_v1.0), Zenodo (2023); <https://doi.org/10.5281/zenodo.7853649>.
54. C. N. McLaughlin, Y. Qi, S. R. Quake, L. Luo, H. Li, Isolation and RNA sequencing of single nuclei from *Drosophila* tissues. *STAR Protoc.* **3**, 101417 (2022). [doi:10.1016/j.xpro.2022.101417](https://doi.org/10.1016/j.xpro.2022.101417) [Medline](#)
55. I. Korsunsky, N. Millard, J. Fan, K. Slowikowski, F. Zhang, K. Wei, Y. Baglaenko, M. Brenner, P. R. Loh, S. Raychaudhuri, Fast, sensitive and accurate integration of single-cell data with Harmony. *Nat. Methods* **16**, 1289–1296 (2019). [doi:10.1038/s41592-019-0619-0](https://doi.org/10.1038/s41592-019-0619-0) [Medline](#)
56. L. Faure, R. Soldatov, P. V. Kharchenko, I. Adameyko, scFates: A scalable python package for advanced pseudotime and bifurcation analysis from single-cell data. *Bioinformatics* **39**, btac746 (2023). [doi:10.1093/bioinformatics/btac746](https://doi.org/10.1093/bioinformatics/btac746) [Medline](#)

57. F. A. Wolf, P. Angerer, F. J. Theis, SCANPY: Large-scale single-cell gene expression data analysis. *Genome Biol.* **19**, 15 (2018). [doi:10.1186/s13059-017-1382-0](https://doi.org/10.1186/s13059-017-1382-0) [Medline](#)
58. D. V. Klopfenstein, L. Zhang, B. S. Pedersen, F. Ramírez, A. Warwick Vesztrocy, A. Naldi, C. J. Mungall, J. M. Yunes, O. Botvinnik, M. Weigel, W. Dampier, C. Dessimoz, P. Flick, H. Tang, GOATOOLS: A Python library for Gene Ontology analyses. *Sci. Rep.* **8**, 10872 (2018). [doi:10.1038/s41598-018-28948-z](https://doi.org/10.1038/s41598-018-28948-z) [Medline](#)
59. F. Supek, M. Bošnjak, N. Škunca, T. Šmuc, REVIGO summarizes and visualizes long lists of gene ontology terms. *PLOS ONE* **6**, e21800 (2011). [doi:10.1371/journal.pone.0021800](https://doi.org/10.1371/journal.pone.0021800) [Medline](#)